1-1-2014

Investigating The Anisotropy Of Magnetic Susceptibility And Other Rock Magnetic Properties Of The Beaver River Diabase In Northeastern Minnesota

Samer H. Hariri
Wayne State University,

INVESTIGATING THE ANISOTROPY OF MAGNETIC SUSCEPTIBILITY AND OTHER ROCK MAGNETIC PROPERTIES OF THE BEAVER RIVER DIABASE IN NORTHEASTERN MINNESOTA

by

SAMER H. HARIRI

THESIS

Submitted to the Graduate School

of Wayne State University,

Detroit, Michigan

in partial fulfilment of the requirements

for the degree of

MASTER OF SCIENCE

2014

MAJOR: GEOLOGY

Approved By:

_____

Advisor Date

DEDICATION

To my parents,

Hussein Hariri and Nadia Barakat,

who continue to work tirelessly, support me, and who had sacrificed many aspects of their lives over the years in order to provide me with the education they were never able to obtain so that I can build a brighter future for myself.

To all my K-12 teachers and college professors, who invested their time in nurturing and teaching me, and who instilled in me a continuous hunger for knowledge and a prodigious curiosity to do science.

To my mentor, Dave Stoddard, who provided me with ample motivation to overcome my personal and academic challenges, and who always encouraged me to be the best that I can be no matter the circumstances.

To my wonderful adviser, Dr. Sarah Brownlee: for her encouragement, generosity, patience, support, and guidance throughout the entire thesis process and my graduate career at Wayne State University.

Finally, I dedicate this work to my future self, as a reminder that with ambition, persistence, and hard work (especially hard work), you can overcome the challenges you will face and reach the goals you set for yourself. Don’t let the small things get in the way; giving up on your dreams is never an option…

ACKNOWLEDGEMENTS

Sincere appreciation and recognition is given to my advisor, Dr. Sarah Brownlee, for her continuous encouragement, generosity, patience, and commitment to guiding me throughout my graduate career. Her insight and methodology has taught me a great deal about the process of being a scientist in the modern world and was an eye opening experience from the beginning. I thank her and Wayne State University for offering me the financial support through the Graduate Research Assistantship which I needed in order to make this research work possible and complete my graduate degree.

I extend my gratitude and appreciation to Dr. Joshua Feinberg from the University of Minnesota in Minneapolis for his contribution and guidance throughout this study. His knowledge and input were very valuable. I also wish to thank the Institute for Rock Magnetism (IRM) for awarding me with the Visiting Research Fellowship which allowed me to use their facility in order to conduct my data acquisition, for which without, this research work wouldn't have been possible. I thank the IRM staff, Michael Jackson, Dario Bilardello, and Peter Solheid for their wonderful dedication and support in helping me configure and run the equipment needed for my data measurements.

The field work portion of this thesis was done using the advice and consultation of Dr. James Miller from the University of Minnesota, Duluth, and Dr. Dean Peterson from Duluth Metals. Their contribution to this work has proven invaluable and I am very grateful and thankful for their input, collaboration, and for providing me with geological maps and field work guidance.

I would like to also thank Wayne State University geology undergraduate students, Mark Baumgardner, Jon Espinoza, and Lauren Schraeder for their invaluable

assistance during field work in Minnesota. Their support, hard labor, contribution, and dedication to this study is admired and meant a lot to me. A thank you is also given to my fellow graduate students, Marty Eakin and Lauren Bugdalski for their encouragement, moral support and friendship during my time at Wayne State.

I would also like to thank my thesis committee members, Dr. Jeffrey Howard and Dr. Lawrence Lemke for their contribution to this thesis and for their patience and availability. Acknowledgement is also given to Gianluca Sperone for assisting me with GIS and the creation of some of the digital maps. I would also like to thank Dr. Sarah Brownlee, Dr. Mark Baskaran, Dr. Ed Van Hees, Dr. Lawrence Lemke, and Dr. Jeffrey Howard, and David Lowrie for making me feel like a part of the WSU geology family and for their amazing support and advice provided throughout my stay at Wayne State University.

Finally, thank you to all my family and friends for your support, patience, and understanding throughout the last few years of my graduate journey.

TABLE OF CONTENTS

LIST OF FIGURES

LIST OF TABLES

CHAPTER 1: INTRODUCTION

Magnetic fabrics in volcanic and shallow intrusive igneous rocks can be a result of various geological processes that may depend on magma flow and deformation subsequent to emplacement (Ellwood, 1978; Hrouda, 1982; Tarling and Hrouda 1993; Canon-Tapia, 2004; Zhang et al 2011). Anisotropy of magnetic susceptibility (AMS) has been used as a tool to study the emplacement mode and deformation history of intrusive igneous rocks. The Beaver River Diabase (BRD) is a series of intrusive dikes and sills in northeastern Minnesota that represent some of the youngest rocks of the Midcontinent Rift System that are exposed. In this study, AMS and other magnetic properties of rocks from the BRD are investigated in an attempt to understand the emplacement and deformation history in the context of the Midcontinent Rift, and to characterize the dominant magnetic carriers of the Beaver River Diabase (BRD).

1.1 Geologic Background

The Midcontinent Rift is a rift system that extends from central Kansas to Lake Superior, and then turns southward into central Michigan. Rocks associated with this system are exposed along the North shore of Lake Superior in Minnesota, and consist of associations of bimodal (felsic and mafic) volcanic, plutonic, and clastic sedimentary units from the 1.0–1.2 Ga old Keweenawan sequence (Morey & Green 1982). The Midcontinent Rift System (MRS) is composed of a lower sequence of predominantly flood basalts and related intrusions, and an upper red bed sequence of largely fluvial sediment, which together have been broadly folded into asymmetric basins due to syndepositional downwarping and late contractional deformation (Van Schmus & Hinze, 1985). Seismic surveys reveal basalt flow thicknesses as great as 20 km in some axial

portions of the rift (Cannon et al 1989). The source of these lava flows is suggested to be melting from an impinging mantle plume that fed the entire rift system during its formation (Hutchinson et al., 1990). The ~1.1 Ga MRS consists of mostly intrusive igneous rocks that were emplaced into co-magmatic volcanic rocks of the North Shore Volcanic Group (Van Schmus & Hinze 1985). The predominance of intrusive igneous rocks in northeastern Minnesota provides a unique look into the late-stage evolution of the MRS. The geochronology of this area suggests that rift development was episodic with magmatism concentrated in short episodes lasting between one and three million years, followed by long periods of inactivity lasting between two to eight million years (Paces and Miller 1993).

The two main intrusive complexes in northeastern Minnesota are the Duluth Complex and the Beaver Bay Complex, which are exposed around the north shore of Lake Superior. The Duluth Complex was emplaced near the unconformity between the earliest basalt flows and the pre-rift basement (Miller and Chandler 1997). Thus, the intrusions in this complex are more deeply seated in the rift system than many other Keweenawan age intrusives, and they display evidence of igneous layering, cumulate textures and mineral foliation (Van Schmus, 1985). The Beaver Bay complex (BBC) covers an area of greater than 600 km^2, and includes intrusions along the Lake Superior shoreline from as far south as Split Rock Point up to Grand Marais at its northern most extension. Furthermore, the BBC extends around 20 km inland, west of the Lake Superior shoreline (Miller & Chandler 1997). Studies from the U.S Geological Survey's COGEOMAP program describe the BBC as being composed of at least 13 major intrusive units that demonstrate various styles of emplacement, a broad range of

parental magma compositions, and unique crystallization histories. Miller and Chandler (1997) suggest that the creation of the BBC is closely related to Graben formation and active volcanism related to the main phase of rifting of the MRS. High precision U-Pb dating of zircons from intrusive rocks in the Duluth complex and BBC suggest periodic intrusive activity in this area between 1.107 and 1.096 Ga (Paces and Miller 1993), which is roughly half the duration of magmatic activity in the MRS, which occurred from 1.109 and 1.086 Ga (Miller and Chandler, 1997). The onset of magmatic activity of the BBC in relation to the Duluth Complex is unknown because attempts to date the oldest intrusive phases of the BBC were unsuccessful (Paces and Miller, 1993).

The Beaver Bay Complex postdates the Duluth complex, and occurs as a cluster of small to medium sized sheet and dike-like intrusions. Most of these thin mafic-to-felsic intrusions formed at medial to shallow levels within the rift succession (Miller and Green, 2002). Magnetic and gravity anomalies associated with this rift system are first-order geophysical features of North America and delineate the extensive nature of rift-related rocks even under thick Paleozoic sedimentary cover (Chase and Gillmer, 1973; Cannon, 1994; Hause, 1996; Hinze, 1997; Stein et al., 2011).

In this study the focus is on the Beaver River Diabase intrusion, and a suite of rock magnetic measurements will be used, including anisotropy of magnetic susceptibility (AMS), high-temperature susceptibility, and hysteresis properties, to better understand the emplacement mechanisms and rifting history preserved within the Beaver Bay Complex (BBC).

The BRD dikes and sills were emplaced into the medial levels of the 6-10 kilometer-thick North Shore Volcanic Group and occur over an arcuate area extending

120 km in length and 20 km in width (Figure 1). The BRD is primarily composed of fine to medium-grained ophitic olivine gabbro rocks. The BBC includes rocks extending from the shoreline at Split Rock Point to Little Marais. The BRD is one intrusion of eleven BBC units. Parental composition of the BRD from Miller and Chandler (1997) show a dominant composition of 48% SiO_2 with up to 10.5% FeO, which is important for rock magnetic studies. The BRD is the most widespread unit of the BBC that is in contact with all the other BBC units as mentioned by Miller and Chandler (1997). In this study, some samples were collected from the southern portion of the BRD as shown in Figure 1. In this region, the outcrops are a part of an originally continuous, nearly horizontal sheet that has locally been eroded. Other samples were collected from the southwestern margin. These outcrops contain continuous dike / dike-like features that dip slightly to the southeast. Samples collected from the Silver Bay region are from the youngest recognized intrusions of the BBC. The outcrops in this region are intermediate in composition. Studies and mapping by Miller (198l), Shank (1989), and Chalokwu and Miller (1992), found that this unit has an in situ differentiation trend that is rich in iron. Within some of the BRD units, there are large inclusions of pure anorthosite that display brecciation and recrystallization textures (Morrison et al., 1983; Miller and Chandler, 1997). Lastly, the wide-ranging intermediate compositions found in several outcrops in the southern region of the BBC suggest derivation from the fractionation of a magma chamber at various stages of differentiation during the formation of the BBC (Miller, 1988; Miller and Chandler 1997).

1.2 Previous Studies

Several petrological and tectonic studies of the BBC have been conducted. However, few studies have investigated magnetic fabrics in certain units of the BBC. The study conducted by Maes et al. (2007) of the Sonju Lake Intrusion used AMS to assess whether magnetic fabric formed as a result of gravitational settling in a fractionating magma chamber, compaction in a dynamic environment after unidirectional flow, or a combination of the two. In a dynamic

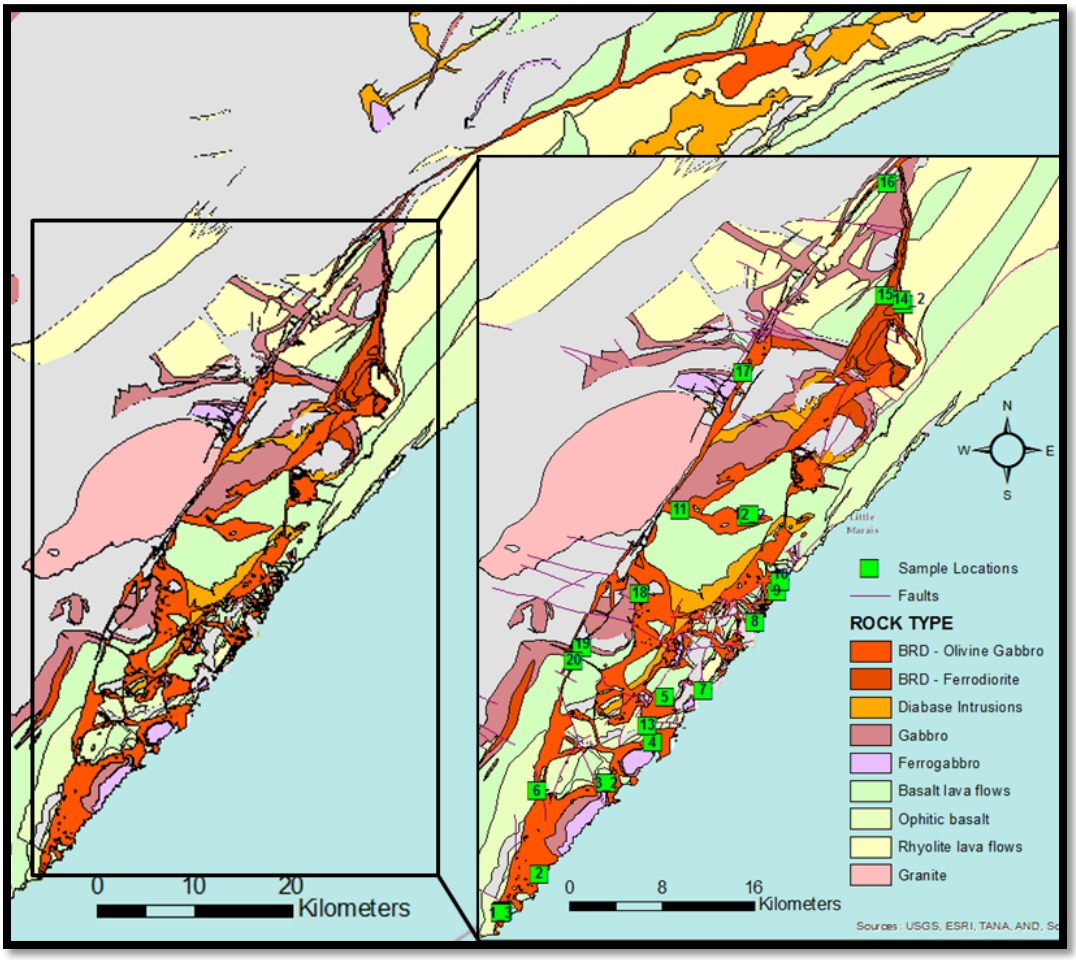

Figure 1. Geologic map showing the Beaver Bay Complex in northeastern Minnesota. The Beaver River Diabase is highlighted in orange. The map also includes a zoomed in view of the area sampled, and sites are marked with green boxes.

environment, such as a crystal laden density flow, a clear lineation is expected to develop (Benn and Allard 1989), while compaction is more likely to generate oblate fabrics, suggesting that both processes took place to some extent. Using AMS and other magnetic properties, such as hysteresis measurements, to investigate the emplacement and flow patterns within the Sonju Lake intrusion, Maes et al (2007) reported the primary source of the magnetic carrier to be a pseudo-single domain (PSD) magnetite or titanomagnetite. In addition, well-aligned magnetic lineations that are consistently plunging shallowly toward the southwest indicate that the source of the magma producing the intrusion is a horizontal sill-like feeder.

The BRD borders parts of the Sonju Lake intrusion, so it is expected that some results, especially those pertaining to prominent magnetic carriers and to a certain extent the source of magma should be similar.

1.3 Objectives & Hypotheses

Based on previous studies, field and geological map observations, a couple hypotheses can be made regarding rocks from the Beaver River Diabase.

1. The magnetic mineralogy in the BRD should be due to magnetite or some variant composition.
2. If the BRD was emplaced through a main feeder dike arc oriented NE-SW, then flow directions in subsequent sills and dikes should be away from the feeder dike, or in SE-NW orientations. In addition, the directions of maximum susceptibility (Kmax) will be used to infer the flow directions.

The goals of this study are two-fold:

1. Characterize the magnetic mineralogy of rocks from the BRD, including their magnetic domain state distribution, using experiments such as magnetic susceptibility as a function of high temperature, and hysteresis parameters.
2. Quantify the magnetic fabric, and attempt to interpret the emplacement and deformation history of the BRD using AMS.

CHAPTER 2: FIELD WORK, SAMPLING, AND SAMPLE PREPERATION

Samples were collected from 20 sites with outcrops belonging to the Beaver River Diabase. The samples were labeled with the prefix BRD, followed by a number indicating which site they were collected from, and another number indicating location within a site when multiple sampling locations were chosen (i.e. BRD_1_1). Four to eight specimens were then drilled from each location at each site. Individual cores were labeled with uppercase letters (i.e. BRD_1_1A). Furthermore, the specimens were cut into several specimens, and a lower case letter was added to the label that indicates what type of measurement the specimen was going to be used for (i.e. BRD-1-1Aa). Table 1 lists the location, number of cores collected, and the rock type of the samples from each site.

Table 1. General site and sample information.

Site Name	Latitude	Longitude	# of Cores	Rock Type
BRD_1_1	47.19998514	-91.38013085	7	Olivine Bearing Gabbro
BRD_1_2	47.19939987	-91.3812707	5	Olivine Bearing Gabbro
BRD_1_3	47.19873304	-91.38247925	5	Olivine Bearing Gabbro
BRD_2	47.21938922	-91.35246309	6	Olivine Bearing Gabbro
BRD_3_1	47.26748075	-91.30089353	5	Olivine Bearing Gabbro
BRD_3_2	47.26745977	-91.29947966	3	Olivine Bearing Gabbro
BRD_4	47.28906234	-91.26327689	5	Olivine Bearing Gabbro
BRD_5	47.31299141	-91.25391889	1	Anorthosite
BRD_6	47.26342813	-91.35367458	1	Olivine Bearing Gabbro
BRD_7	47.31686957	-91.22404466	6	Olivine Bearing Gabbro
BRD_8	47.352945	-91.18386477	6	Olivine Bearing Gabbro
BRD_9	47.36913596	-91.16706986	4	Olivine Bearing Gabbro
BRD_10	47.3741306	-91.16428713	6	Olivine Bearing Gabbro
BRD_11	47.41197534	-91.24215154	7	Olivine Bearing Gabbro
BRD_12_1	47.40866026	-91.19045975	5	Olivine Bearing Gabbro
BRD_12_2	47.4094067	-91.18815421	8	Olivine Bearing Gabbro
BRD_13	47.29828646	-91.26806746	6	Olivine Bearing Gabbro
BRD_14_1	47.52075703	-91.06771836	6	Rhyolite?
BRD_14_2	47.52290121	-91.06947283	8	Olivine Bearing Gabbro
BRD_16	47.58420605	-91.0806785	6	Olivine Bearing Gabbro
BRD_17	47.48460595	-91.19324182	6	Olivine Bearing Gabbro

BRD_18	47.36806441	-91.27423433	6	Olivine Bearing Gabbro
BRD_19	47.33951177	-91.31900957	7	Olivine Bearing Gabbro
BRD_20	47.33244214	-91.3253756	7	Olivine Bearing Gabbro

2.1 Sampling Locations

Fieldwork was conducted the week of May 2nd, 2013. Financial and time constraints did not allow for a complete sampling of the entire extent of the BRD, and thus the area studied was the southern half of the BBC as shown in Figure 1. The area studied is located in the southern portion of Lake County and part of the southwestern portion of Cook County in Minnesota, and spans along the shoreline from the city of Two Harbors in the southwest near Split Rock Lighthouse State Park, to near Temperance River State Park in the northeast, and inland to the cities of Silver Bay and Finland. (Figure 1)

Samples were collected from BRD outcrop locations determined using geologic maps provided by James D. Miller, from the University of Minnesota in Duluth, and from digital maps provided by Dean Peterson from Duluth Metals. In addition, several road maps and a GPS device were used in order to determine the locations of many of these outcrops.

A total of 20 sites were sampled. Ten sites were at or near the Lake Superior shoreline on the eastern boundary of the BRD, five were on the western boundary of the BRD, and the remaining five were scattered in-between. Most of the sites along the shoreline were exposed from road cuts along Minnesota State Highway 61 and were easy access on the side of the road, while others were more difficult to get to and had to be accessed by foot.

2.2 Sampling Methods

Major field equipment, including a drill and core orienter, was borrowed from the Institute for Rock Magnetism at the University of Minnesota in Minneapolis. Oriented cylindrical core samples were collected using a water-cooled drill (Pomeroy EZ Core Drill Model D261-C) with a 1-inch diameter diamond drill bit (Pomeroy BSS-1E). Cores were drilled to between 2 and 4 inches long. Cores were oriented using a standard paleomagnetic core orienting apparatus (Pomeroy Orienting Fixture) as shown in Figure 2. The orienting fixture was used to measure the trend and plunge of the 1-inch in-place drilled cores. It uses a Brunton compass and an attached vertical protractor for angle measurement. When possible, trend azimuth was additionally measured using a sun compass attached to the apparatus to account for inaccuracies caused by local magnetic fields. After drilling, the core sample usually remains attached at the base, and must be removed using a special, non-magnetic, brass chisel. Before detaching the core, we place the orienting apparatus into the hole, and level the Brunton compass by rotating and adjusting the angle. A copper wire was used to mark the top of the core by placing it through a slot in the tube and dragging it along the top of the core. For cases when the core broke during drilling, we oriented the empty drill hole. Before drilling the actual core sample, a shallow mark was made by the drill bit so that broken cores can be re-oriented after the hole has been oriented (Figure 3). To avoid miss-orientation of the core after removal, an arrow is drawn on the side of the core pointing out of the hole to indicate the surface of the outcrop (Figure 4). The core is then labeled and packed in a sample bag along with other cores from the same site. We sampled 20 sites, with 4 to 7 cores per site.

Figure 2. Student Lauren Schraeder orienting a drilled sample using the Pomeroy Orienting Fixture with a Brunton Compass installed.

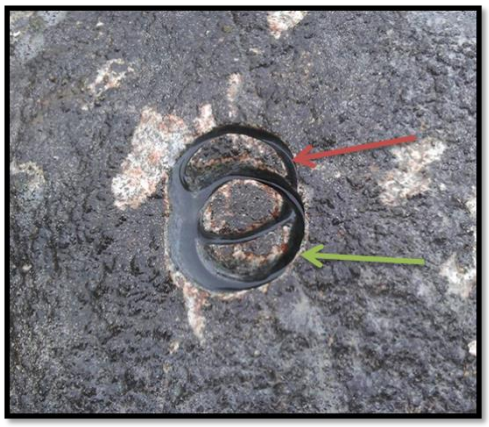

Figure 3. Red Arrow: Drill mark used to allow for proper orientation if drill core breaks. Green arrow: Actual drill core.

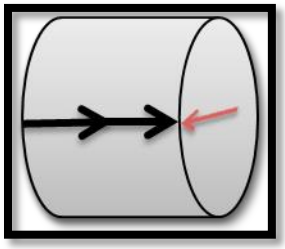

Figure 4. Illustration of a one inch diameter and length cylindrical core sample. Black arrows point toward the surface of the outcrop, red arrow points up

2.3 Sample Preparation

Measurements of all magnetic parameters, including AMS, hysteresis properties, and high temperature susceptibility were conducted at the Institute for Rock Magnetism (IRM) at the University of Minnesota in Minneapolis, and were made possible through a Visiting Fellowship awarded to Samer Hariri for this study. Samples were prepared accordingly for each type of measurement and will be discussed in the subsections below. The samples were cut and prepared at the IRM. Detailed information pertaining to the magnetic properties measured and details regarding the instruments used will be discussed in later chapters of this document. The following subsections only describe how samples, for each magnetic property and the specified instruments, were prepared.

2.3.1 Anisotropy of Magnetic Susceptibility (AMS) Sample Preparation

For AMS measurements conducted using the Geofyzika KLY-2-KappaBridge and the Roly-Poly Bridge, the one-inch core samples were cut into one inch length cylindrical cores (Figure 4). Effort was made to have the deepest end of the cores be cut rather than those closer to the surface of the outcrop to avoid near surface weathering, but some samples were not as long as others and had to include portions that were closer to the surface. The mass of all samples was then measured.

Another arrow (red in Figure 4) was marked on the top surface of the specimen such that it is perpendicular to the field arrow and pointing toward the direction of that arrow (where the core was scribed in the field), essentially, this arrow points up on this surface. The red arrow is used in determining the position of the sample when placed in the holder of both instruments.

2.3.2 Vibrating Sample Magnetometer (VSM) Sample Preparation

For VSM measurements using the Princeton Measurements micro-VSM (hot) instrument, the core samples were cut into thin disks roughly 1 cm in length. The samples were then properly labeled with the specimen name. Effort was made to use a deeper part of the original core for this measurement, again to avoid near-surface weathering. For these measurements, only one specimen from each site was chosen as representative of the entire site, and not all core specimens from the site were used.

2.3.3 High Temperature Susceptibility Sample Preparation

For high temperature susceptibility measurements using the Geofyzika KLY-2-KappaBridge (in Curie temperature mode), one representative specimen from each site was used. A small chip of the specimen, anywhere between 1 and 5 grams was crushed into smaller chips, and powdered so that it could be inserted into a small test tube which would be inserted into the furnace attachment of the instrument. The test tubes were marked with the name of each specimen.

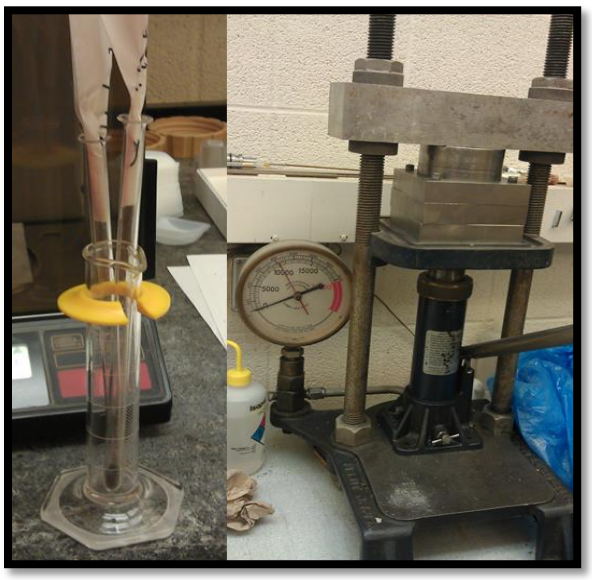

Figure 5. Left: High Temperature specimens in test tubes. Right: High pressure crushing apparatus.

CHAPTER 3: MAGNETISM & ANISOTROPY OF MAGNETIC SUSCEPTIBILITY

3.1 Introduction

It is known that magnetic properties are a result of moving charges. On the atomic level, electrons orbiting a nucleus of an atom are similar to a current (I) flowing through a conducting loop. The current will induce a magnetic field, H, specific to the loop. This magnetic field is mathematically described as the ratio of the current divided by the diameter (d) of the loop.

$$H = I/d \qquad (3.1)$$

This gives the loop an intrinsic magnetic strength that is called the magnetic moment, m, over the area (A) of the loop.

$$m = IA \qquad (3.2)$$

The intensity of this magnetization (M) is thus equivalent to the magnetic moment per unit volume (V).

$$M = m/V \qquad (3.3)$$

3.2 Classes of magnetic materials

When magnetic fields are applied to materials, such as rocks, the electron spins produce a magnetization that opposes the original field that created it. Following this premise, it can be said that all materials are magnetic or can exhibit some form of magnetism. However, some materials will be more magnetic than others. The level at which materials become magnetized depends on the overall magnetic moments

produced at the atomic level. The variation in magnetization levels and of magnetic behavior divides materials into the following five groups:

1. Diamagnetic

   Diamagnetic materials exhibit weak magnetic behavior. The atoms in diamagnetic materials have no net magnetic moments because all of their electrons are paired. When immersed in an external magnetic field, the magnetic moments of these materials will align antiparallel, or opposite to the external field, thus they have a negative magnetization.

2. Paramagnetic

   Paramagnetic materials have unpaired electrons in partially filled orbitals, and thus can have some net magnetic moment. When immersed in an external field, partial alignment of magnetic moments will occur parallel to the field, but the magnitude of such alignments is small and thus will still be considered to be weak and the materials to be nonmagnetic. Both diamagnetic and paramagnetic materials will lose their magnetizations when the external field is turned off.

3. Ferromagnetic

   Ferromagnetic materials exhibit electric force interactions that produce parallel alignment of magnetic moments that are strong and very prominent. The magnetic moments can align even in the absence of an external magnetic field. This is known as spontaneous magnetization. When immersed in a high field, ferromagnetic materials reach a maximum magnetization known as saturation magnetization. The magnetization does not increase beyond the maximum no matter how large the external field gets.

4. Antiferromagnetic

Antiferromagnetic materials will exhibit magnetic moments in their crystal lattices that are equal but opposite to one another, resulting in a net moment of zero. Some moments, however, might be slanted or tilted and thus result in a small net magnetization of the material. Such materials are called canted antiferromagnetic, and hematite is a classic example of a canted antiferromagnetic material.

1. Ferrimagnetic

Ferrimagnetic materials have complex crystal structures and molecular ordering that results in multiple magnetic sublatices. This is common in ionic compounds such as oxides. The electric force interactions are negated by oxygen ions in between the magnetic lattices. These interactions result in variation in the magnitude of the magnetic moments, resulting in a net magnetic moment. Ferrimagnetic materials behave exactly like ferromagnetic ones, except that in ferrimagnetic materials, while the moments are antiparallel to one another, they have different magnitudes, resulting in a net magnetic moment.

Ferrimagnetic materials have small regions between 10^{-6} and 10^{-4} m (larger than atomic scale of ~10^{-10} m) called magnetic domains. The magnetization in each domain may not be parallel to its neighboring domain, which is why ferrimagnetic materials have varying magnetic moments.

The domain state of materials depends on the grain size of that material. If the grain size is very small, then the magnetic moment of that grain will be uniform and point in one direction. However, as the grain size increases, energies associated with

the charge distribution will affect the electric forces, and thus create multiple sources of magnetic fields, creating two or more moments in one grain. This effect is referred to as the magnetostatic energy. However, to maintain the separations of magnetic moments within one grain, domain walls are created, and they require energy as well, which is referred to as wall energy. As a result of the balance between magnetostatic and wall energy, grains will not be infinitely divided into multiple domains. The size of the grain determines the number of domains that will be created (Dunlop, 1981; Tarling and Hrouda, 1993; Dunlop and Ozdemir, 1997).

There are four magnetic domain states:

1. Superparamagnetic (SPM) refers to grains of magnetic materials that are too small to form a true and stable magnetic domain, and thus behave as paramagnetic.
2. Single Domain (SD) refers to grains of magnetic material that are small enough to include only one magnetic domain, but large enough to have a stable domain.
3. Psuedo-Single Domain (PSD) refers to grain sizes that are slightly larger than single domain, but one domain is dominant, so the behavior is similar to single domain.
4. Multidomain (MD) refers to large grain sizes that include many magnetic domains. Because domain walls, once created, are relatively easy to move, magnetism held in multi-domain materials is constantly changing by realigning with the external field.

Domain states can be determined using hysteresis properties, which will be discussed in Chapter 4. In addition to domain state, magnetic behavior is also dependent on temperature. Effects of temperature will be discussed in Chapter 5.

3.3. Magnetic susceptibility

Before AMS is introduced in this chapter, it is important to describe the concept of magnetic susceptibility. The magnetic susceptibility (often known as the bulk magnetic susceptibility, χ_b) is a parameter used to describe how materials behave magnetically when immersed into a uniform, usually low frequency magnetic field. Mathematically, magnetic susceptibility is the ratio of the induced magnetization (M_i) and the external magnetic field (H). This makes χ_b a unitless parameter when volume normalized, or have units of m^3/kg when mass normalized.

$$M_i = \chi_b H \qquad (3.4)$$

Magnetic susceptibility can be used as a tool to extract information regarding the composition of a rock sample, since all minerals within a rock contribute to the bulk magnetic susceptibility. It is a relatively quick method to investigate magnetic fabric, grain size, domain states, and mineralogy of rocks (Tauxe 2008). At the atomic level, magnetic susceptibility is a result of the response of electronic orbits and/or unpaired electron spins to an applied magnetic field. The diamagnetic component is usually weak when measuring magnetic susceptibility, whereas the paramagnetic component is strong. If there are trace amounts of ferrimagnetic minerals in a rock, then the ferrimagnetic component will dominate the magnetic susceptibility. In highly magnetic minerals, such as magnetite, the susceptibility is dominated by shape anisotropy, where the shape of the grain determines the direction of easy magnetization. A sphere has no

shape anisotropy, where a needle would have high shape anisotropy, with preferred magnetization direction parallel to the long axis of the needle. Shape anisotropy produces a maximum susceptibility parallel to the long axis, because that's where all the magnetic moments align at saturation (Tauxe 2008).

3.4 Anisotropy of Magnetic Susceptibility

The anisotropy of magnetic susceptibility (AMS) is a measure of the directional dependence of a rock's response to an external magnetic field, and is frequently used as a measure of the shape preferred orientation of the magnetic minerals within a rock, because AMS is usually dominated by shape anisotropy (Tarling and Hrouda, 1993). The variation of susceptibility based on orientation can be mathematically described as a second-order tensor that can be presented as a three-dimensional ellipsoid.

AMS is a useful tool for measuring intrinsic properties of petrofabrics, and can provide more detailed interpretations than bulk susceptibility on its own. The interpretation of AMS results proves troublesome when used alone because of the variation of magnetic properties with mineralogy and grain size. It is therefore important to combine AMS with information on composition, grain size, and other geologically relevant information to make reasonable geological interpretation of magnetic fabric.

There are three types of AMS, magnetocrystaline, stress, and shape. Magnetocrystaline anisotropy depends on the preferred direction of the electron spins in the crystal lattice of magnetic minerals. Strain anisotropy is related to spin-orbit coupling which arises from the strain dependence of anisotropy constants. Shape anisotropy depends on the shape of the magnetic mineral grains. The magnitude of AMS depends on the anisotropy of the minerals and their alignment within a rock. Unfortunately, AMS

is not able to distinguish one from the other. One reason why the interpretation of AMS is difficult is because the shape anisotropy of magnetic grains can differ depending on the domain state. Thus, other magnetic properties such as hysteresis and high temperature susceptibility aid in the interpretation of AMS results.

3.5 Calculation of AMS

The susceptibility tensor in AMS is calculated using a least squares technique (Girdler 1961, Janak 1965, Jelinek 1977, Hanna 1977). When a low external magnetic field (<1mT) is applied to a magnetically anisotropic sample, the magnetization, M, is not parallel to the applied field, H, and its three perpendicular parts can be written as:

$$\begin{aligned} M_1 &= \chi_{11}H_1 + \chi_{12}H_2 + \chi_{13}H_3 \\ M_2 &= \chi_{21}H_1 + \chi_{22}H_2 + \chi_{23}H_3 \\ M_3 &= \chi_{31}H_1 + \chi_{32}H_2 + \chi_{33}H_3 \end{aligned} \qquad (3.5)$$

The coefficients χ_{ij} are the elements of the second order tensor that is the AMS tensor. Thus using subscript notation we get:

$$M_i = \chi_{ij} H_j \qquad (3.6)$$

This is also expressed as a matrix:

$$\chi_{ij} = \begin{pmatrix} \chi_{11} & \chi_{12} & \chi_{13} \\ \chi_{21} & \chi_{22} & \chi_{23} \\ \chi_{31} & \chi_{32} & \chi_{33} \end{pmatrix} \qquad (3.7)$$

where $\chi_{12} = \chi_{21}$, $\chi_{23} = \chi_{32}$, and $\chi_{31} = \chi_{13}$

3.6 AMS Methods

Different methods can be used to measure AMS. In this study, the 15-position scheme was adopted from Jelinek, 1977 (Figure 6). The measurements were conducted at the Institute for Rock Magnetism, at the University of Minnesota, in Minneapolis. The susceptometer used was the Geofyzika KLY-2 KappaBridge AC Susceptibility Bridge. In addition, some samples were measured using the “Roly-Poly” Magnetic Anisotropy Bridge, an in-house designed AMS bridge that uses stepper motors that rotate the sample at 1.8 degree increments in three orthogonal planes, and provides a total of 600 directional susceptibility measurements from which the best-fit AMS tensor is obtained by least squares fitting. This device was only used for samples that had higher magnetizations because those with low values of magnetization showed considerably large error ellipses.

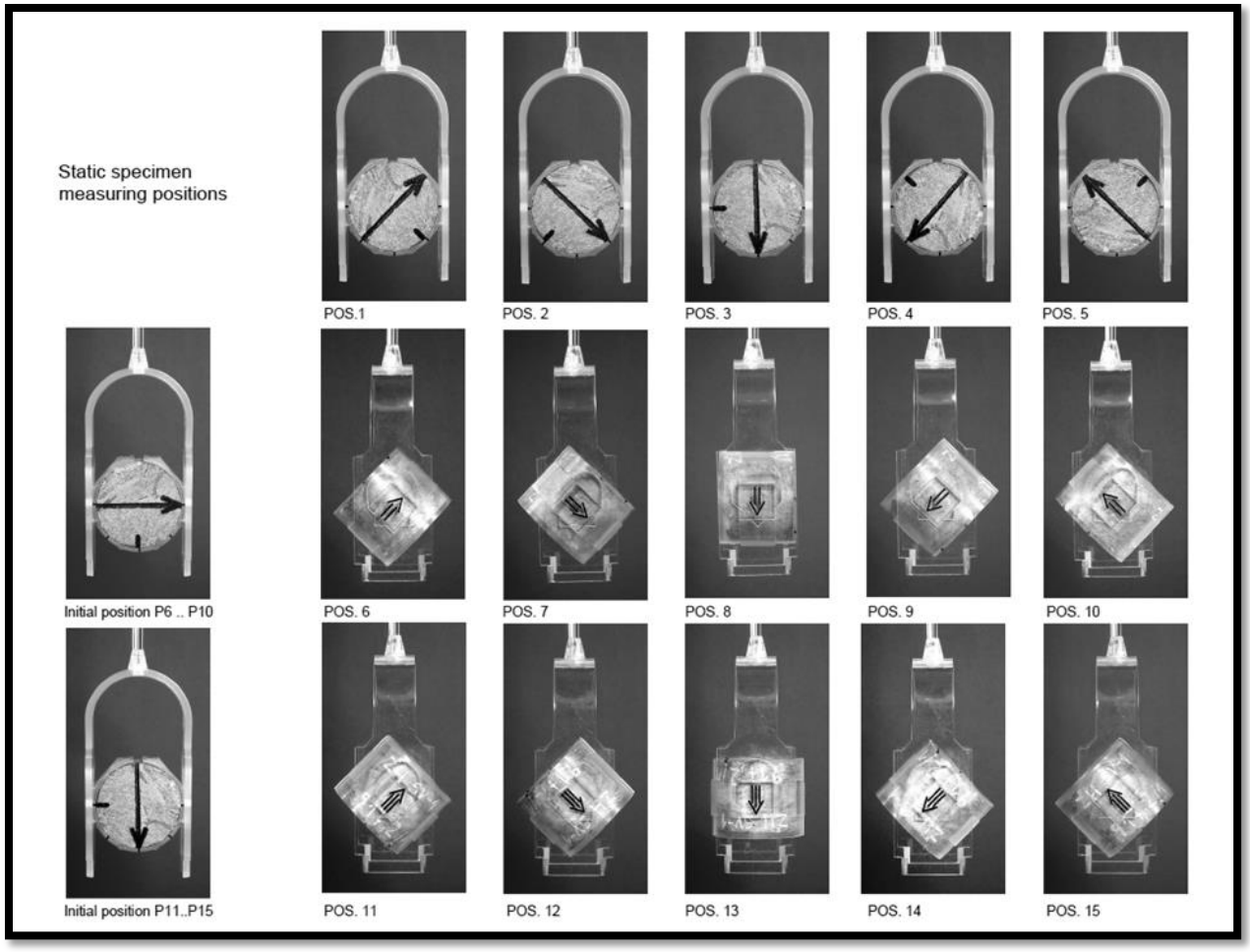

Figure 6. The 15 position AMS measuring sequence taken from Jelinek 1987. Image source: AGICO MFK1 User Guide.

The AMS tensor can be represented by a three-dimensional ellipsoid that has maximum (κ_{max}), intermediate (κ_{int}) and minimum (κ_{min}) directions, each orthogonal to one another. The mean value of the susceptibility is given by κ_{mean}, where $\kappa_{mean} = (\kappa_{max} + \kappa_{min} + \kappa_{int}) / 3$.

Characterization of the magnetic fabric uses ratios of pairs of the principle axes. Of these, Balsey and Buddington (1960) proposed the lineation ratio:

$$L = \kappa_{max}/\kappa_{int} \qquad (3.8)$$

Stacey (1960) used the foliation ratio:

$$F = \kappa_{int}/\kappa_{min} \quad (3.9)$$

In this study, the parameters devised by Woodcock (1977) were used to calculate the lineation and foliation axial ratios. Here, the natural log of the ratios L and F are taken:

$$L' = \ln (L) \quad (3.10)$$

$$F' = \ln (F) \quad (3.11)$$

This adaptation allows for slightly easier interpretation of the AMS data.

Nagata (1961) proposed the Anisotropy Degree, P where:

$$P = \kappa_{max}/\kappa_{min} \quad (3.12)$$

Owens (1974) suggested the use of a "Total" anisotropy parameter, A, where:

$$A = (\kappa_{max} - \kappa_{min})/ \kappa_{mean} \quad (3.13)$$

Today, the most studies use the corrected Anisotropy parameter, P_j, by Jelinek 1981 where:

$$P_j = e\sqrt{2[(\eta_1 - \overline{\eta})^2 + (\eta_2 - \overline{\eta})^2 + (\eta_3 - \overline{\eta})^2]} \quad (3.14)$$

where $\eta_1 = \ln \kappa_{max}$; $\eta_2 = \ln \kappa_{int}$, $\eta_3 = \ln \kappa_{min}$, and $\overline{\eta} = (\eta_1 + \eta_2 + \eta_3)/3$.

The corrected degree of anisotropy incorporates the intermediate and mean susceptibility rather than just the maximum and minimum values, making it a more informative parameter than P or A. In addition, it expresses the magnetic properties using logarithmic values of susceptibility.

The shape factor parameter, T (Jelinek, 1981), can be used to determine the shape of the ellipsoid, and it combines lineation and foliation parameters, thus including all three principal susceptibilities in its calculations.

$$T = (2\eta_2 - \eta_1 - \eta_3) / (\eta_1 - \eta_3) \quad (3.15)$$

These parameters provide useful relationships that can be used to analyze AMS results. Various plotting conventions are used in the literature; most common are the Flinn, Ramsay, and Jelinek diagrams (Figure 7). The Flinn diagram plots the lineation and foliation ratios, F vs L after Flinn (1962). The Ramsay diagram (Ramsay, 1976) is similar except that it has the advantage of having a minimum value of zero on both axes as opposed to 1 on the Flinn diagram. The Jelenik diagram plots the corrected anisotropy (P_j) vs. the shape factor (T) after Jelinek (1981).

The Flinn and Ramsey diagrams are polar plots, where the radial trajectory from the origin indicates increasing anisotropy, and the shape is reflected in the angle above or below the radial trajectory such that the shape is oblate if below the line, and prolate above it. However, only points that lie along the plot axes (F or L) are ever truly oblate or prolate, and the rest of the plot is in the “triaxial” region, meaning all three principal axes are different from one another.

The Jelenik diagram is Cartesian, where the corrected anisotropy increases along the x-axis, and the shape factor along the y-axis. Points that lie above the x-axis (positive T values) are considered oblate, whereas those that lie beneath the x-axis (negative T values) are prolate. Again, it is often practiced that only those points that have values of T=1 or T=-1 can be considered truly oblate or prolate, with anything falling in between considered triaxial.

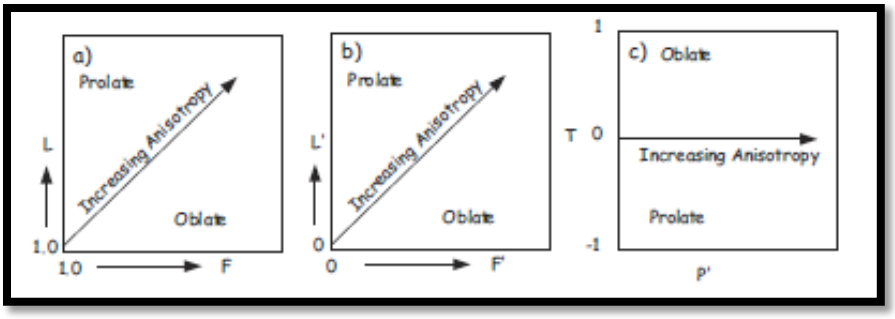

Figure 7. Examples of graphs used in analysis of AMS data. a) Flinn Diagram b) Ramsey Diagram c) Jelenik Diagram. Source: Adopted from Tauxe, 1998.

In addition to the above plots, Tauxe et al, (1998) used a ternary projection plot that uses three axes as shown in figure 8. The projection plots the normalized eigenvalues τ_1, τ_2, and τ_3 and when $\tau_1 > \tau_2 > \tau_3$, the projection area is limited to the bottom right of the ternary diagram as shown in Figure 8 below. The projection can then be plotted as a normal x-y plot using the parameters of Elongation (E') and Roundness (R) , as devised by Tauxe 1998, where:

$$E' = \tau_1 + 0.5\,\tau_3 \qquad (3.16)$$

and

$$R = \sin(60°)\,\tau_3 \qquad (3.17)$$

In addition, the ternary projection provides one more bit of information, and that is the percent anisotropy (%h) devised by Tauxe in 1990. The percent anisotropy increases on a diagonal slope downward as shown in figure 8.

$$\%h = 100(\tau_1 - \tau_3) \qquad (3.18)$$

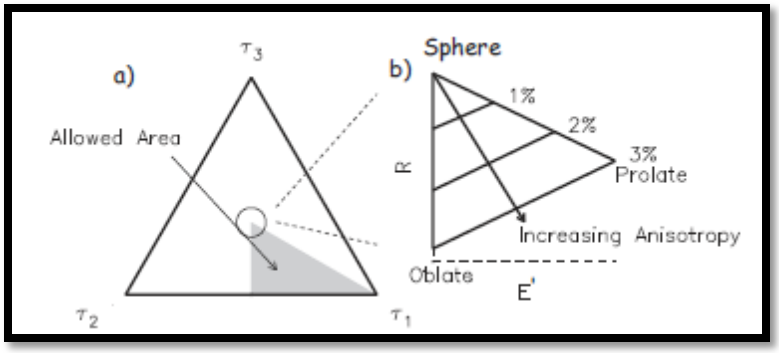

Figure 8. Example of Ternary diagram. a) There are three axes with limits of τ_1, τ_2, τ_3. Data falls into the shaded triangle.
b) Zoomed in area showing how diagram can be plotted using elongation, E', and roundness (R).

3.7 Results

The Ramsay, Jelinek, and Ternary Projection (Figures 10, 11, and 12) all show that most of the data is triaxial, with the exception of sample BRD 11, which shows a more oblate shape and also has the highest percent anisotropy. The specimens collected from site 1, BRD 1-1, 1-2, and 1-3 have similar degrees of anisotropy and percent anisotropy, but differ in shape such that BRD 1-1 is triaxial, BRD 1-2 somewhat triaxial, and BRD 1-3 having a significant increase in its shape factor towards oblate. At this location, the outcrop was a sill in the center that turned into a dike on the southern end as shown by a change in orientation of columnar joints in Figure 9. It can be thus speculated that samples collected from sill like structures might be more oblate in shape than those from dikes.

Figure 9. Site BRD 1-1 outcrop. At southern margin (to the left), columnar joints are tilted due to the transition from sill (vertical columns) to dike (horizontal columns)

AMS results from the BRD are shown in Tables 2, 3, and 4. The mean values of the susceptibility ranges from 1881 x 10^{-6} to 43833 m^3/kg. Sites with the highest susceptibilities include 14-2, and 16-1, and that with the lowest is 8-1. The percent anisotropy values ranged from 0.42% to 13.16%. The highest of these values is from site 11-1, and the lowest is from site 14-1. Ten sites had values less than 1%, eight had values between 1% and 2%, and the remaining six had values greater than 3%. These six sites are 17-1, 16-1, 14-2, 9-1, 15-1, and 11-1 respectively.

Table 2. AMS Mean Values and Eigen Values.

Site	$\kappa_{max, mean}$	$\kappa_{int, mean}$	$\kappa_{min, mean}$	Mean Susceptibility κ	T_1	T_2	T_3
1-1	26431.28571	26169.74286	25869.82857	26156.97143	0.336829323	0.33349633	0.329674347
1-2	24886.26	24728.3	24505.4	24706.66	0.335756522	0.333625382	0.330618095
1-3	18234.92	18151.98	17869.08	18085.3	0.33609051	0.334561831	0.329347659
2-1	26646.43333	26333.35	25880.73333	26286.85	0.337893213	0.333923123	0.328183664
3-1	16965.722	16680.166	16133.68	16593.19	0.340816979	0.33508057	0.324102451
3-2	9697.97	9570.543333	9248.953333	9505.823333	0.340071231	0.335602859	0.32432591
4-1	10434.416	10210.712	10000.732	10215.28	0.340483706	0.333184058	0.326332235
6-1	18135.2	17895.4	17265	17765.2	0.340275745	0.335776312	0.323947943
7-1	10459.37	10396.24167	10321.70667	10392.42167	0.335480104	0.333455288	0.331064608
8-1	1930.7425	1893.1425	1819.3025	1881.0625	0.342136869	0.335473968	0.322389164
9-1	8908.08	7725.8475	6940.09	7858.015	0.377877042	0.327727232	0.294395726
10-1	8233.408333	8167.256667	8079.485	8160.045	0.336329979	0.333627722	0.3300423
11-1	20374.74286	19355.42857	13384.40571	13384.40571	0.383599832	0.364408974	0.251991194
12-1	8010.708	7914.04	7867.002	7930.584	0.336701083	0.332637994	0.330660922
12-2	7795.355714	7743.257143	7674.28	7737.63	0.335820088	0.333575707	0.330604205
13-1	5710.886	5629.64	5533.932	5624.814	0.338433744	0.333619012	0.327947244
14-1	8009.253333	7962.195	7908.125	7959.858333	0.335401861	0.333431209	0.33116693
14-2	47768.62857	43753.94286	39977.61429	43833.37143	0.36325902	0.332729134	0.304011847
15-1	18345.99	15344.714	13696.97	15795.894	0.387146877	0.323812348	0.289040775
16-1	34144.9	31736.33333	29680.95	31854.08333	0.357305566	0.332101384	0.31059305
17-1	9311.735	8838.325	8362.465	8837.498333	0.351220225	0.333364136	0.315415638
18-1	7617.4725	7500.0725	7335.105	7484.215	0.339268305	0.334039523	0.326692172
19-1	15248.06	14780.88714	14518.29	14849.08857	0.34228969	0.331802556	0.325907754
20-1	9196.25	9126.636	9011.55	9111.48	0.336434598	0.333887848	0.329677554

Table 3. Fischer mean values for declination and inclination. Also showing the alpha 95% value.

Site	Declination	Inclination	Alpha (95%)	n
1-1	164.2	57.5	22	7
1-2	98.7	59.2	30.3	5
1-3	108.1	54.9	46.4	5
2-1	83	74.1	39.5	6
3-1	24.7	36	64.3	6
3-2	341.8	64.3	104.6	4
4-1	338.7	73.1	86.4	5
6-1	339.5	78.8	0	2
7-1	276.1	45	84.1	6
8-1	351.3	58.1	37.5	5
9-1	353.9	76	89.7	4
10-1	53.7	36.7	62	7
11-1	320.6	33	42.1	7
12-1	308.9	51.1	36.9	6
12-2	233.2	66.4	64.2	7
13-1	285.6	58.9	41.9	5
14-1	330.7	81.9	89.7	6
14-2	95.7	51.7	43	7
15-1	355.7	57.1	82.1	5
16-1	98.9	72.7	40.4	6
17-1	43.7	39	72.2	6
18-1	69.2	79.5	102.1	5
19-1	350.7	81	36.5	8
20-1	182.4	82.1	88.6	5

Table 4. AMS parameters.

Site	Ln L (L')	Ln F (F')	Pj	T	Percent Anisotropy (h)	Elongation (E')	Roundness (R)
1-1	0.009944483	0.011526521	1.018626106	0.073682543	0.715497655	0.501666497	0.285506359
1-2	0.006367507	0.009054835	1.013235328	0.174249024	0.513842695	0.50106557	0.28632367
1-3	0.004558791	0.015707801	1.017310932	0.550117615	0.67428512	0.50076434	0.285223439
2-1	0.011819111	0.017337392	1.025143986	0.189264134	0.970954836	0.501985045	0.284215391
3-1	0.016974607	0.033311336	1.043480263	0.324876673	1.671452834	0.502868205	0.280680956
3-2	0.013226607	0.034179587	1.040880019	0.441988236	1.5745321	0.502234186	0.280874477
4-1	0.021672208	0.020779075	1.037539283	-0.021039015	1.415147103	0.503649824	0.282612006
6-1	0.013311104	0.035862366	1.042440157	0.458606259	1.632780192	0.502249717	0.280547148
7-1	0.006053865	0.007195242	1.011439783	0.086147458	0.441549629	0.501012408	0.286710361
8-1	0.019666497	0.039784961	1.051587816	0.338401517	1.974770464	0.503331451	0.279197206
9-1	0.142387205	0.107256783	1.246199183	-0.140722082	8.348131582	0.525074905	0.254954178
10-1	0.008066993	0.010804938	1.016253901	0.145080288	0.628767934	0.501351129	0.285825016
11-1	0.051323112	0.36888265	1.433723824	0.755723901	13.16086378	0.509595429	0.218230776
12-1	0.012140749	0.005961348	1.016624015	-0.341363857	0.604016098	0.502031545	0.286360759
12-2	0.006705717	0.008947941	1.013465408	0.143239629	0.521588218	0.50112219	0.286311641
13-1	0.014328681	0.017146903	1.027382914	0.089536774	1.048649977	0.502407366	0.284010645
14-1	0.005892824	0.006814004	1.010982865	0.072494831	0.42349305	0.500985326	0.286798975
14-2	0.087787387	0.090262077	1.166445295	0.013898889	5.924717325	0.515264943	0.263281982
15-1	0.178639972	0.113596409	1.298031701	-0.222571749	9.810610244	0.531667264	0.250316654
16-1	0.073151047	0.066956761	1.129711284	-0.04421086	4.671251581	0.512602091	0.268981472
17-1	0.052178054	0.055344139	1.097266726	0.029445878	3.58045867	0.508928044	0.273157956
18-1	0.015531935	0.022240961	1.03272033	0.177614824	1.257613244	0.502614391	0.28292372
19-1	0.031117345	0.017925703	1.045095968	-0.268980873	1.638193627	0.505243567	0.282244394
20-1	0.007598621	0.012690083	1.017369689	0.250950572	0.675704448	0.501273375	0.285509137

3.8 Discussion

The magnetic anisotropy will be greatly influenced by the composition of a sample. Sites that showed the highest percent anisotropy definitely suggest the presence of ferrimagnetic minerals, such as magnetite (and more precisely a variation of titanomagnetites as shown in the results section of the high temperature susceptibility measurements, Chapter 5). Those with lower anisotropy and susceptibility values indicate small amounts of ferrimagnetic components.

The directions of all the samples maximum and minimum axes are shown in Figure 13. The AMS data can be split into three categories based on the orientation of their AMS principal axes: a group that is representative of dike or dike like features, a

group that is sills, and a group that is dike turning into sill. Plotting the declination/inclination of κ_{min} data onto stereonets provides us with a visual identification of dikes/sill features. The grouping is based on the assumption that minimum AMS directions are perpendicular to magma flow directions, so κ_{min} should be perpendicular to intrusion walls (i.e. horizontal for dikes and vertical for sills). This assumption may break down at the margins of these intrusions, a phenomenon known as inverse magnetic fabric (Borradaile and Jackson, 1992). We first plotted the κ_{min} directions for each site, and then based on the mean values of the minimum axes, the sites were separated into the three categories mentioned. After the separation, bootstrap statistics were performed to "clean" the data and it shows quite nicely the differences between sites that are from dike features, than those that are from sill.

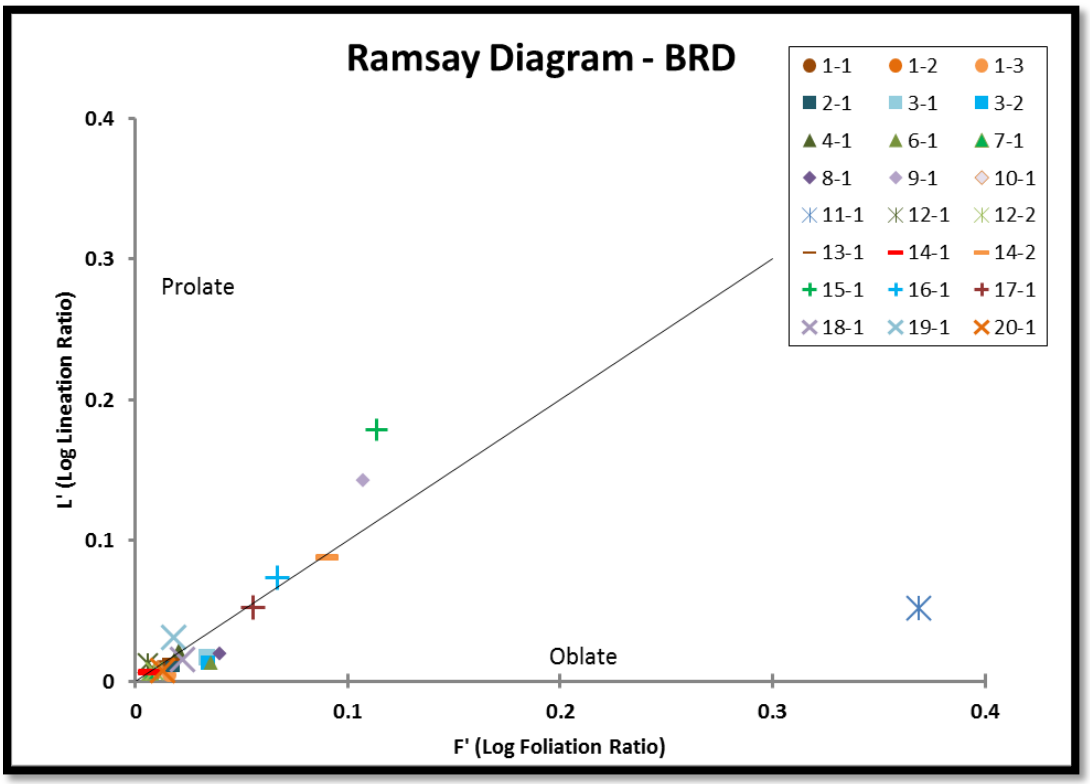

Figure 10. Ramsey diagram showing most samples to be triaxial except for one which is oblate.

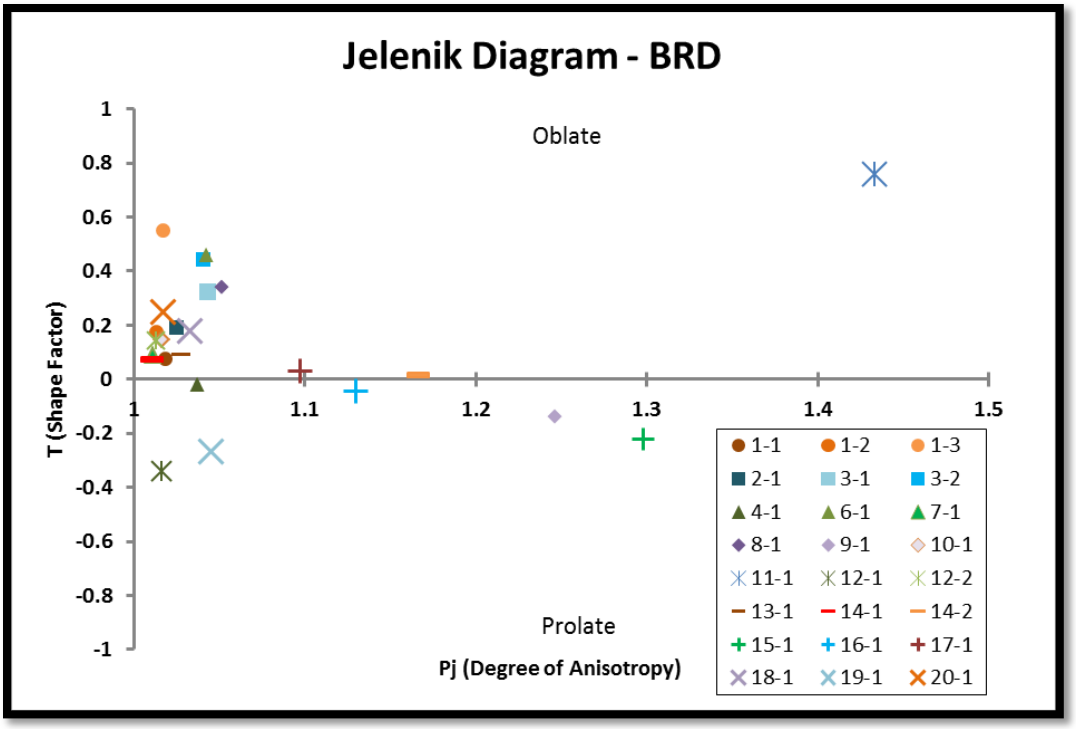

Figure 11. Jelenik diagram showing shape factor and degree of anisotropy.

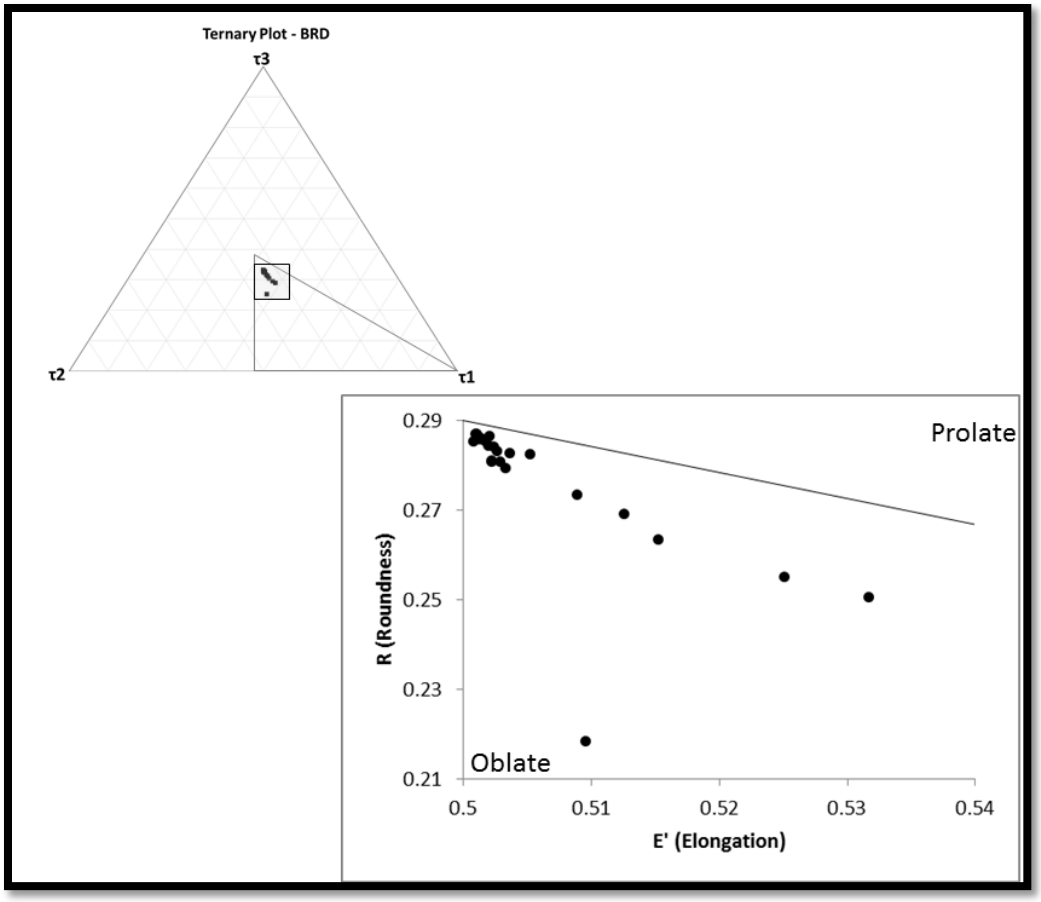

Figure 12. Ternary diagram (top) projected on an Elongation/Roundness plot (bottom). Sample 11-1 is the oblate outlier in this figure. Percent anisotropy increases to the bottom.

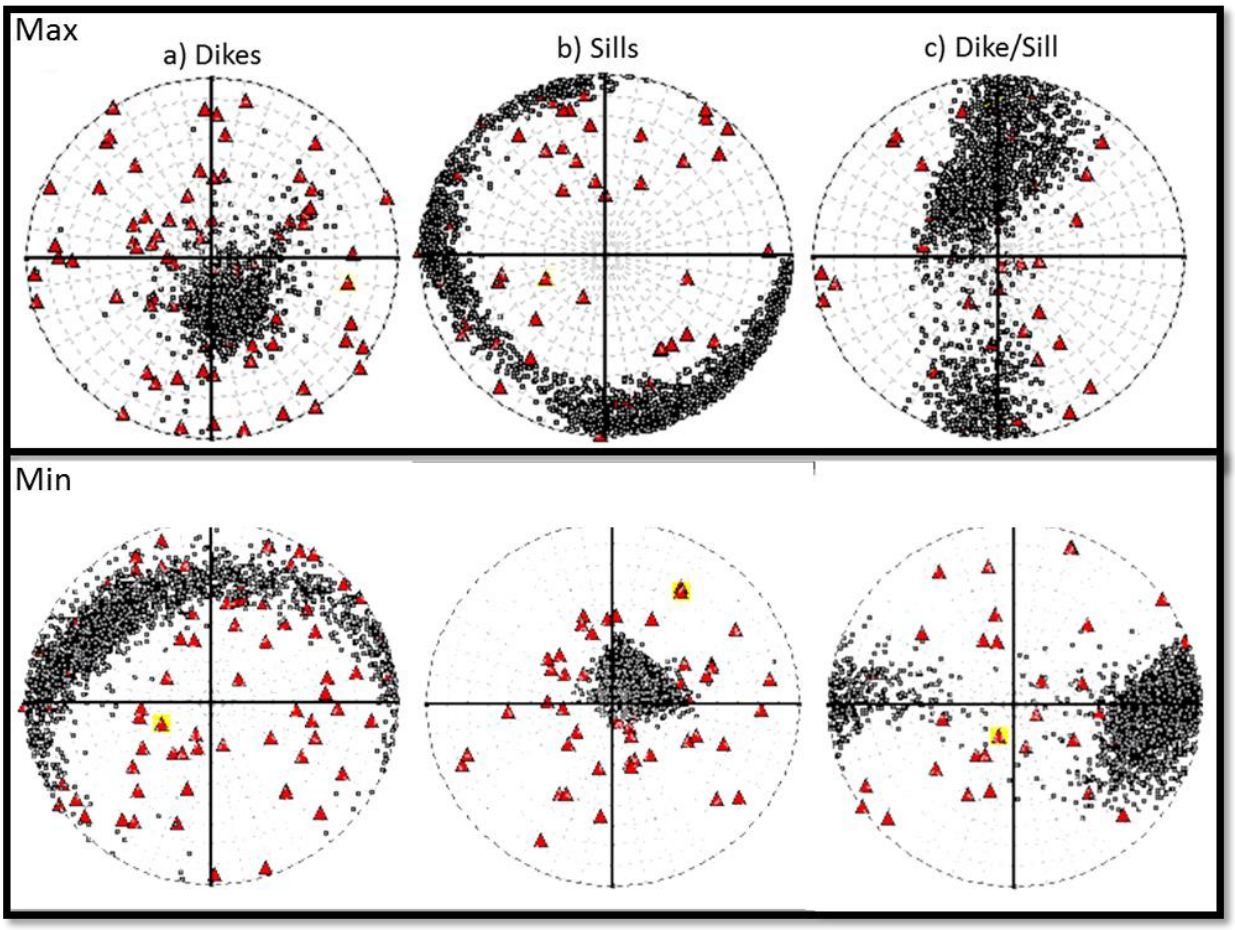

Figure 13. Bootstrap statistic stereonets for BRD samples. Top: maximum AMS inclination and declination values. Bottom: Minimum AMS inclination and declination values. a) Congregation of points in the middle (max) and on the edges (min) suggest dike features with a slight SE flow. b) Congregation of points around the edges (max) and in the middle (min) suggests sill features. c) Points have no clear congregation, perhaps features are somewhere in between dikes and sills. Red triangles are data points from Table A1, black dots are bootstrap extrapolation with N=2000.

CHAPTER 4 – HYSTERESIS PROPERTIES

4.1 Introduction

Ferromagnetic and ferrimagnetic materials that are immersed in an external magnetic field will retain a memory of that field once it is turned off. This is called remenance, and results in a property called hysteresis, where the magnetization of a sample in an increasing applied field follows a different path when the applied field is decreased. The full path of magnetization as the applied field is first increased, then decreased, reversed, and increased again is called a hysteresis loop. There are several useful parameters that arise from hysteresis measurements that can be used to infer sample grain size and domain state. These parameters are shown in Figure 14. The saturation magnetization (M_s) is the maximum magnetization value obtained when the applied external field reaches 1 T or more. When the applied external field is reduced back to zero, there is a remenant magnetization (M_r) left in the material. When the field turns negative, the magnetization will reach zero at an applied field value known as the coercivity of the material (H_c). Finally, the coercivity of remenance (H_r) is the point where the reverse field reduces the remanence magnetization to zero after the field is applied and then removed.

The saturation magnetization and the coercivity can be related to grain size as shown in Figures 15 and 16 (Dunlop & Ozdemir 2007). The reduced saturation of remanence is the ratio of the remanent magnetization to the saturation magnetization. When plotted against the reduced remanent coercivity (the ratio of the coercivity of remanence to the coercivity), information pertaining to the domain state can be established (Day et al., 1977). This is referred to as the Day plot. The Day plot shows

the domain state of a material based on the ratios mentioned above. For grains that are single-domain (SD), the M_r/M_s ratio is greater than 0.5 and an H_{cr}/H_c ratio of 2 or less. For pseudo-single domain (PSD), M_r/M_s ranges between 0.1 and 0.5, while H_{cr}/H_c ranges between 2 and 4. For multi-domain (MD), $M_r/M_{s\ is}$ less than 01 and H_{cr}/H_c is greater than 4. For SPM (Superparamagnetic state), $M_r/M_{s\ is}$ a lot less than 0.01 while H_{cr}/H_c is greater than 10 (Day et al. 1977).

Values for H_c vary for each domain state. For magnetite, SD grains can be anywhere between 10 and greater than 40 mT, PD range between 10 and 15 mT, while MD are less than 10 mT.

From the relationship between grain size and hysteresis parameters, the domain state of a grain can be determined by the shape of a hysteresis loop. For example, loops that have high M_r and high H_c (typical of SD) will be wider than those for MD. Figure 17 shows examples of some of the shapes hysteresis loops can have for SD and PSD states. MD assemblages and theoretical behaviors of Mr/Ms and Hcr/Hc ratios are seen in Figure 18.

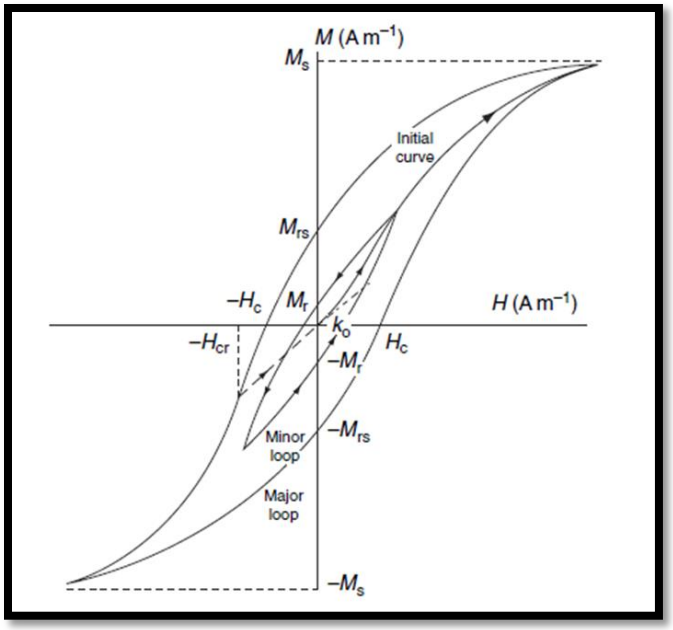

Figure 14. Hysteresis Loop Example from Dunlop & Ozdemir 2007. Note: In this document Mr refers to the remanent magnetization instead of Mrs.

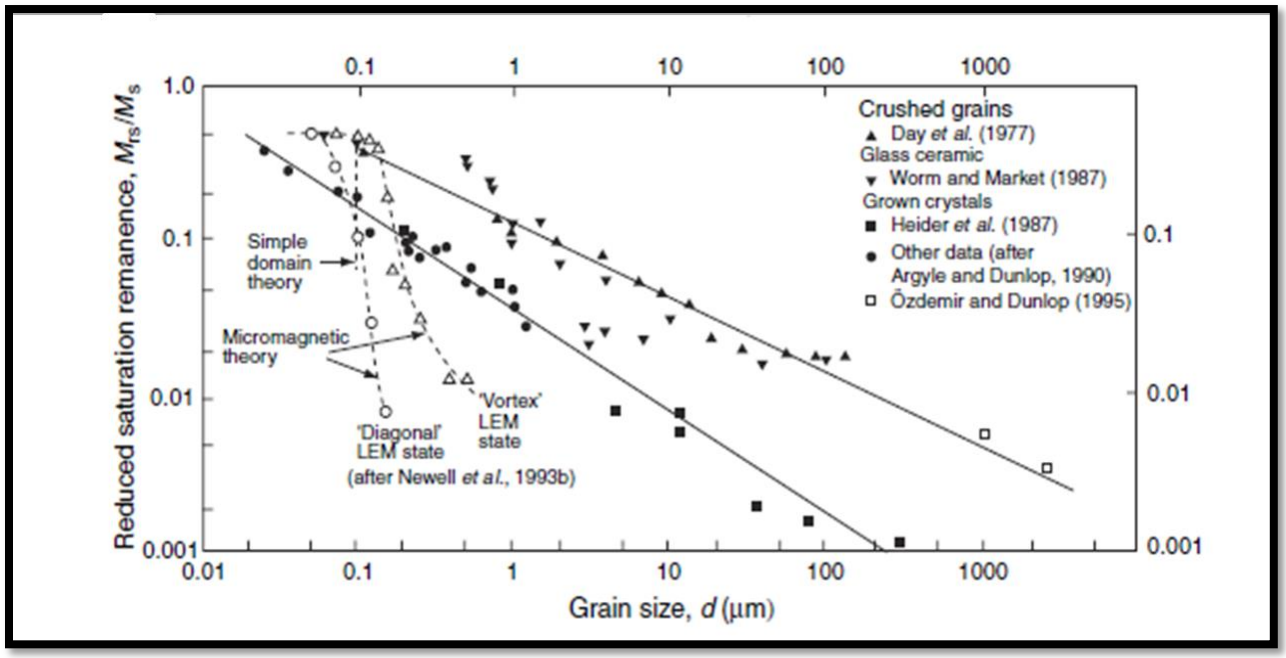

Figure 15. Mr/Ms ratio against grain size. (Dunlop & Ozdemir 2007)

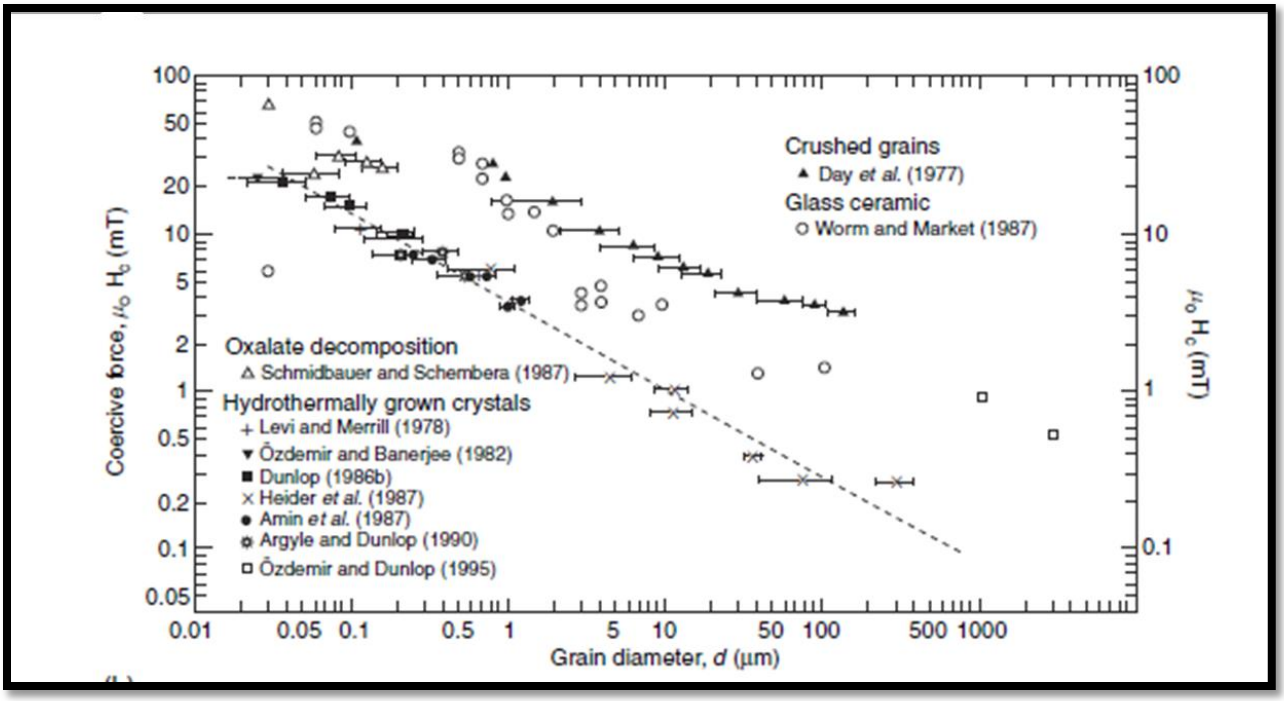

Figure 16. Coercivty against grain size. (Dunlop & Ozdimeer 2007).

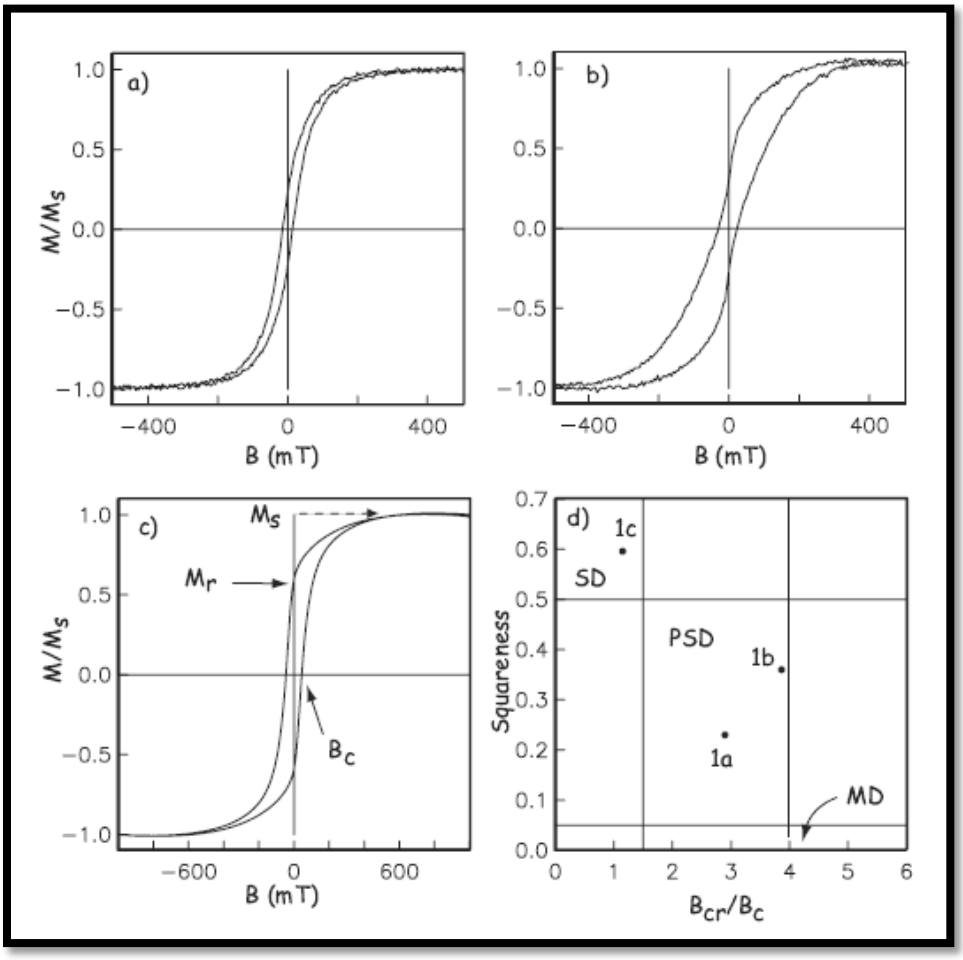

Figure 17. Three examples of shapes hysteresis loops can have. a) Potbelly shape indicative of PSD state. b) Wasp-waisted shape indiating two magnetic mineral dominance and PSD. c) Elongated potbelly with high Mr indicating SD. d) Day plot for all three examples. (Tauxe et al 2002).

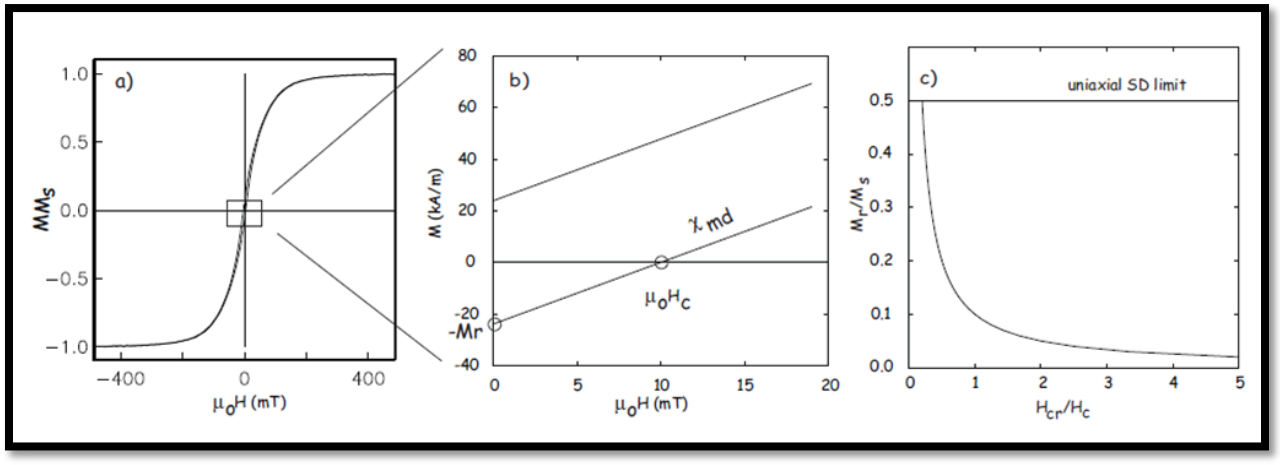

Figure 18. a) MD shape of hysteresis loop. b) Zoomed in on box to show theoretical behaviour of Hc. c) Theoretical relationship between Mr/Ms and Hcr/Hc. (Tauxe et al 2014).

4.2 Methods

Hysteresis properties were measured at the IRM using the Princeton Vibrating Sample Magnetometer (Hot) apparatus. The sample was attached to a plastic rod, and fixed to the vibrating rod on the top of the instrument. The sample was then calibrated such that it would be aligned at its geometric center relative to where the two coils that will produce the applied external field were located. After alignment is achieved, the instrument will vibrate the sample at a relatively high frequency and apply a changing magnetic field to a maximum value of 1 T. The field was then reduced to zero, and then increased to -1T, back to zero, and then to 1T, and finally back to zero. Measurements of the sample's magnetization were taken every 20 mT. These measurements are then used to construct hysteresis loops for each sample.

4.3 Results

The samples were divided into 5 categories (A to E) first based on their saturation magnetization values, and second on the coercivity value. Samples had low saturation magnetizations (less than 0.3 Am^2/kg), medium (0.4-0.6 Am^2/kg) or they had high saturation magnetizations (greater than 0.6 Am^2/kg). In addition, the saturation magnetization may be used to infer grain size (Figure 15): lower magnetizations indicate small grain size, and higher magnetizations indicate larger grain size. Saturation magnetization however may also be related to the amount of magnetic material present within a sample.

The coercivities vary with magnetization, there doesn't seem to be a relationship between the coercivity of a specimen, and its magnetization value (Figure 19).

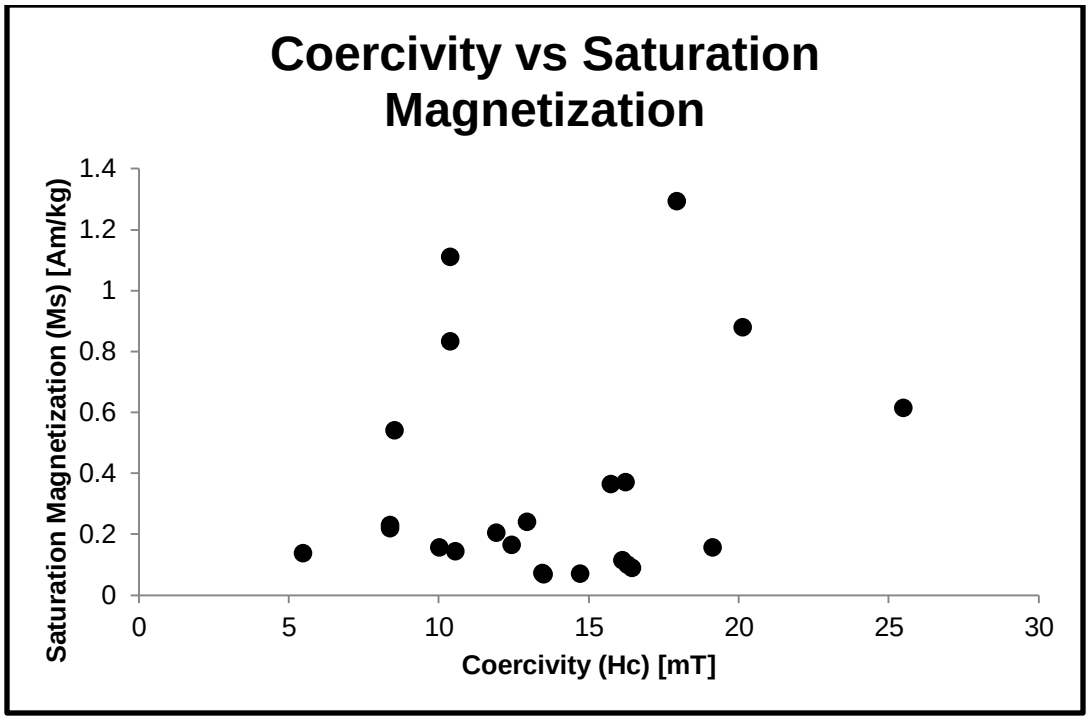

Figure 19. No apparent correlation between M_s and Coercivity.

All hysteresis loops, for the most part, have a semi-potbellied shape with coercivity ranges between 5 and 27 mT (Figure 20). This suggests the presence of a PSD magnetite, or some variant of magnetite, as the dominant magnetic carrier in samples from the BRD. Categories A and B appear to have a low percentage of magnetite, whereas categories D and E have the highest percentages of magnetite present in the samples, and category C is somewhere in between. Table 5 shows the results of some the parameters. Refer to Appendix B for complete set of hysteresis loops done for this study.

The Day plot (Figure 21) shows that most samples are PSD, while very few are MD. This is typical of natural samples and infers that the grain size of the magnetic carriers of most of these samples ranges between 0.1 to 20 microns.

Table 5. Hysteresis properties of sites from the BRD.

Sample	Ms [Am/kg]	Mr [Am/kg]	Bc [mT]	Bcr [mT]	Bcr/Bc	Mr/Ms
BRD-1-1Fd	0.538557	0.07085	8.53266	28.73	3.367062557	0.131555249
BRD-1-2Ed	1.1095	0.101719	10.3889	39.92	3.842562735	0.091680036
BRD-1-3Bd	0.217991	0.0175848	8.39866	36.2	4.310211391	0.08066755
BRD-2-1Bd	0.830588	0.0761487	10.3889	39.92	3.842562735	0.091680472
BRD-3-1Ad	0.228214	0.0184094	8.39865	36.2	4.310216523	0.080667268
BRD-4-1Dd	0.155127	0.0151512	10.0258	39.2	3.909912426	0.097669651
BRD-6-1Ad	0.613661	0.131523	25.5075	63.49	2.489071842	0.214325173
BRD-7-1Bd	0.2379	0.0286	12.95	51.1	3.945945946	0.120218579
BRD-8-1Bd	0.0865746	0.0113225	16.4665	49.94	3.032824219	0.130783163
BRD-9-1Ad	0.0698306	0.00789565	13.4721	59.44	4.412081264	0.113068626
BRD-10-1Ad	0.0683693	0.00956462	14.7382	49.55	3.362011643	0.139896415
BRD-11-1Dd	0.361943	0.0799615	15.7448	29.47	1.871729079	0.220922908
BRD-12-2Ad	0.154734	0.02695	19.1353	46.49	2.429541214	0.174169866
BRD-13-1Dd	0.136321	0.00720498	5.489	34.65	6.312625251	0.052853045
BRD-14-1Cd	0.16225	0.020773	12.4438	40.98	3.293206255	0.128030817
BRD-14-2Fd	0.3686	0.0633	16.25	52.49	3.230153846	0.171730874
BRD-15-1Ad	0.0986957	0.0173797	16.3055	44.09	2.703995584	0.176093791
BRD-16-1Ad	0.877133	0.15969	20.1445	46.65	2.315768572	0.182059049
BRD-16-1Dd	1.29178	0.212978	17.9531	45.48	2.533267235	0.164871727
BRD-17-1Bd	0.112798	0.0228961	16.1451	32.2	1.994413166	0.202983209
BRD-18-1Cd	0.141263	0.0147664	10.5625	46.42	4.394792899	0.104531264
BRD-19-1Cd	0.203612	0.0235103	11.9342	44.85	3.758106953	0.115466181
BRD-20-1Bd	0.0661529	0.00905699	13.5115	44.4	3.286089627	0.136909947

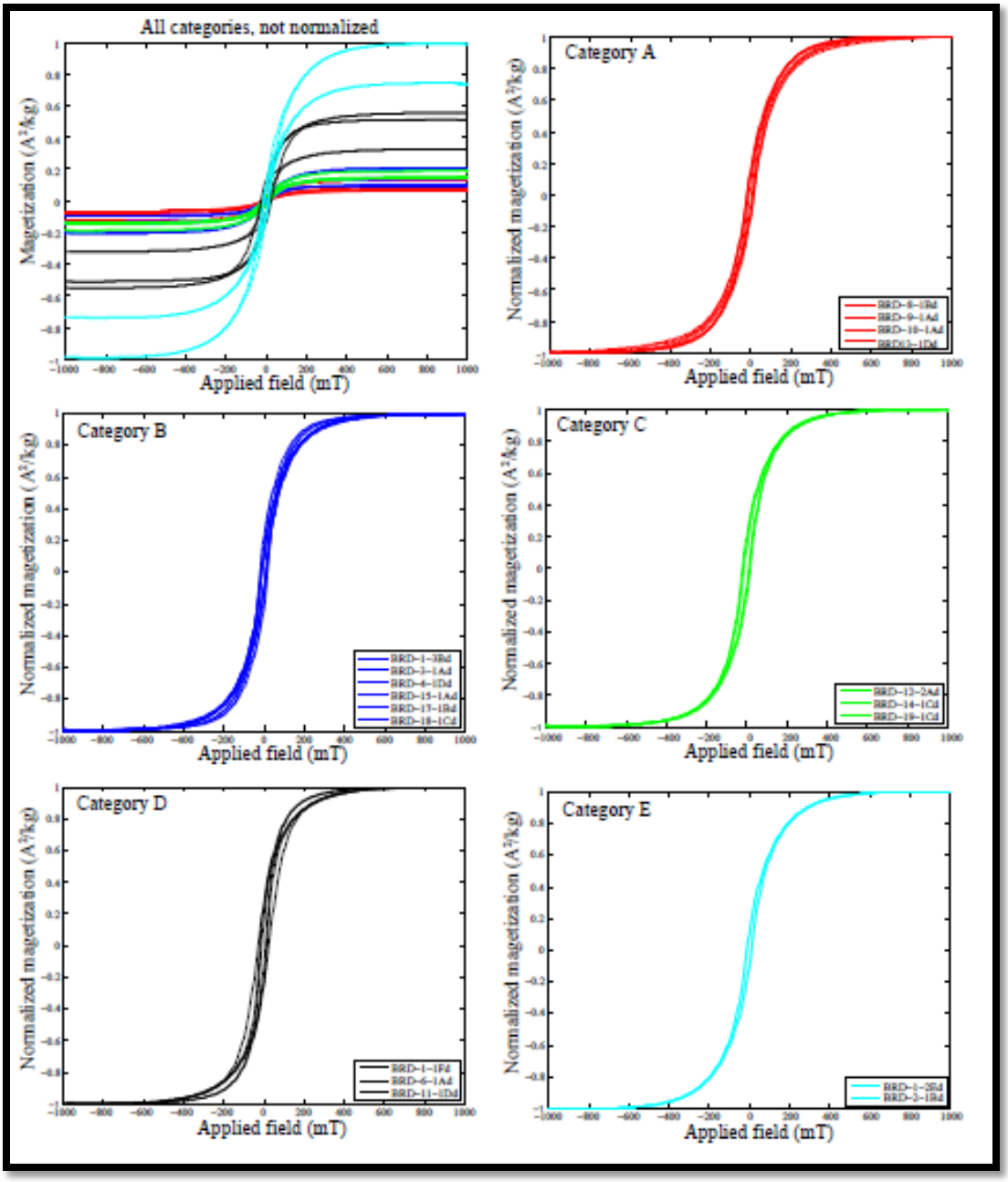

Figure 20. Hysteresis loops normalized to show differences in shape.

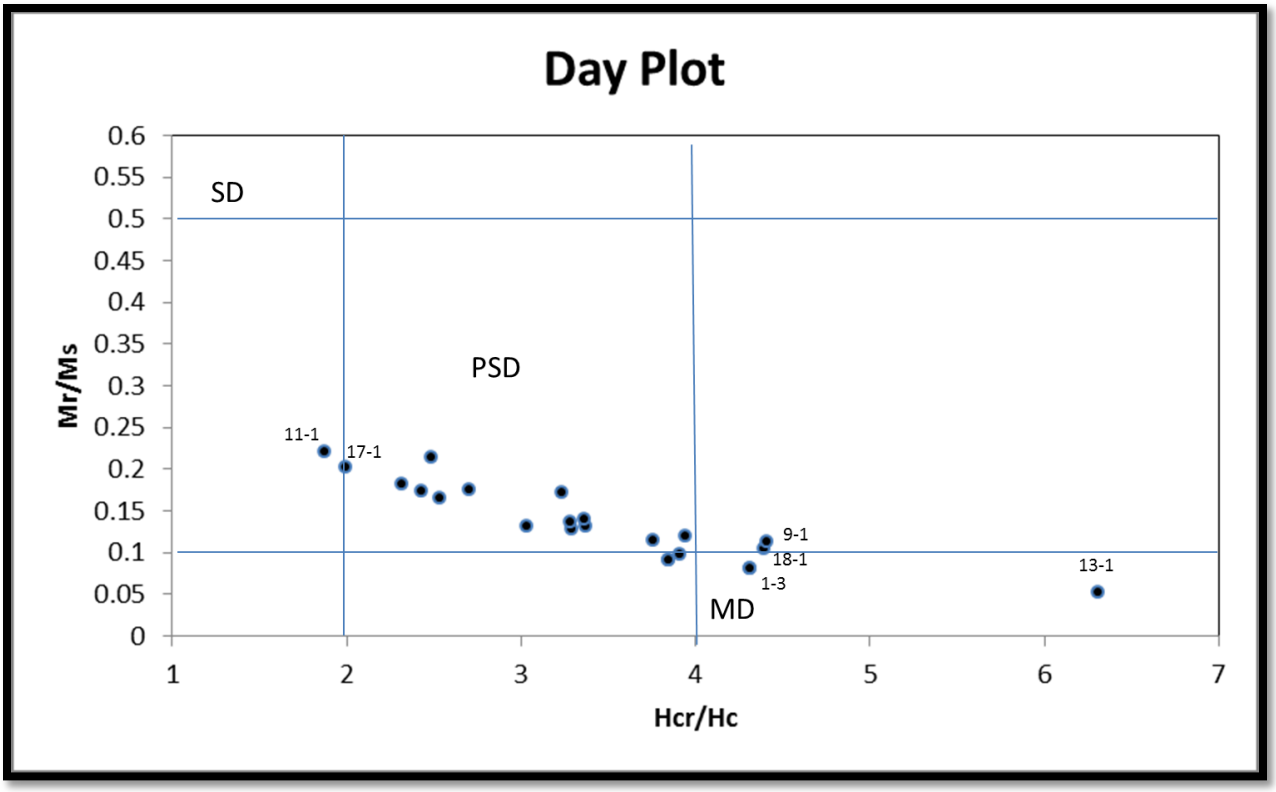

Figure 21. Day plot showing the domain states of BRD samples. Most fall under the PSD state.

4.4 Discussion

The overall shape of the hysteresis loops is mostly uniform across all categories. While there are differences in the saturation magnetization and coercivities, they all indicate magnetite, or some form of magnetite, as the dominant magnetic mineral. Appendix B shows all the plots of these hysteresis loops. Differences in M_s of each category are likely related to different proportions of magnetite present at each site, as well as the grain size of the magnetic minerals.

CHAPTER 5 – HIGH TEMPERATURE SUSCEPTIBILITY

5.1 Introduction

The magnetic susceptibility of a material is temperature dependent, especially in ferromagnetic and ferrimagnetic materials. The alignment of magnetic moments ceases at certain temperatures when the thermal energy is greater than electromagnetic energy. This is defined as the Curie temperature. Below the Curie temperature, the magnetic moments are aligned and considered to be ordered. Once the Curie temperature is reached, the magnetic moments become randomized, and the material loses its magnetic properties. Each material has an intrinsic Curie temperature, thus Curie temperature can be used to identify mineralogy of samples. However, various minerals may have similar curie temperatures; therefore additional information for mineralogical identification would be needed for more accurate magnetic mineral identification.

In iron oxides such as magnetite, the iron can be substituted by titanium (Nagata, 1961). The electron spin configuration of titanium is different than in iron, thus magnetite with titanium substitution ratios (titanomagnetite) will experience different magnetic properties than pure magnetite. Figure 18 (Buttler, 1992; Tauxe et al., 2014) is a ternary diagram for iron oxides showing how titanium substitution changes magnetite into ulvöspinel.

Titanium substitution causes exsolution in magnetite grains. Diffusion of cations through magnetite crystals creates bands within a grain that are either titanium rich or titanium poor. This creates a change in the grain size of the crystal, which affects the magnetization and may alter the domain state of the magnetic grain (Feinberg 2005,

Tauxe et al 2014). Figure 19 shows a microscopic image of a magnetite crystal undergoing exsolution and having its grain size reduced. As discussed in chapter 4, smaller grain sizes allow for magnetization in one direction, while larger grain sizes allow for PSD and MD states. From this, it can be assumed that the more titanium rich a mineral is, the smaller the effective grain size. However, it should be noted that many titanomagnetite do not show exsolution. Furthermore, its domain state would be closer to single domain than not.

The curie temperature of titanomagnetites depends on the ratio of titanium substitution. Data from O'rielly (1984) show the relationship between curie temperatures and titanium substitution ratios (Figure 20).

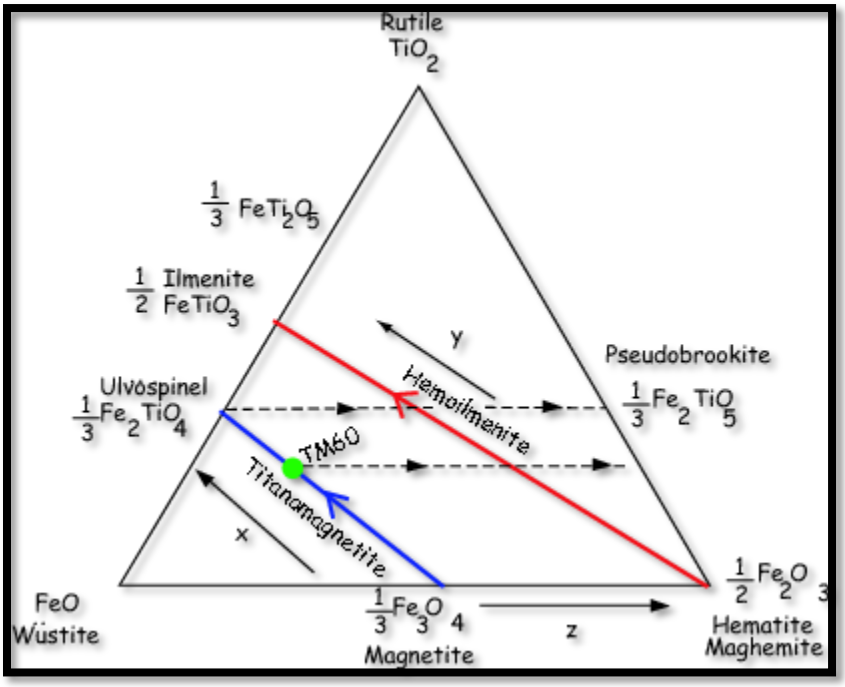

Figure 22. Terenary diagram of iron oxides from Buttler (1992) and Tauxe et al. (2014).

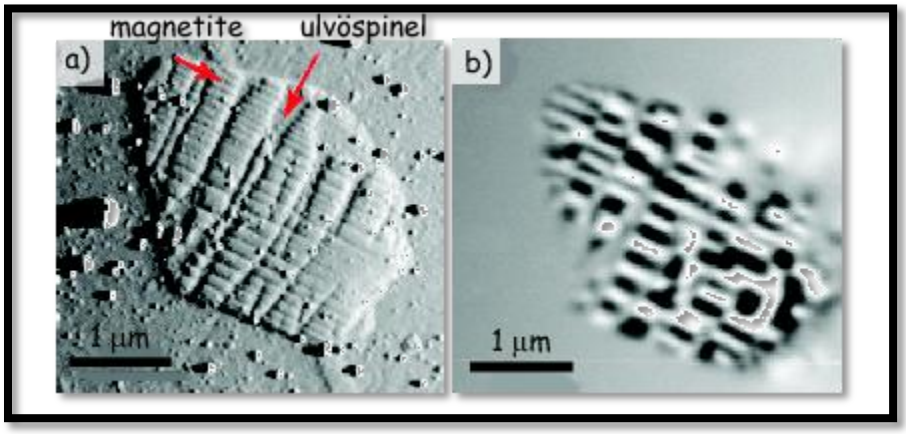

Figure 23. Microscopic images of a magnetite grain (a and b) showing how titanium substitution and subsequent exsolution of ulvöspinel affects magnetization and domain states. (Fienberg et al , 2005)

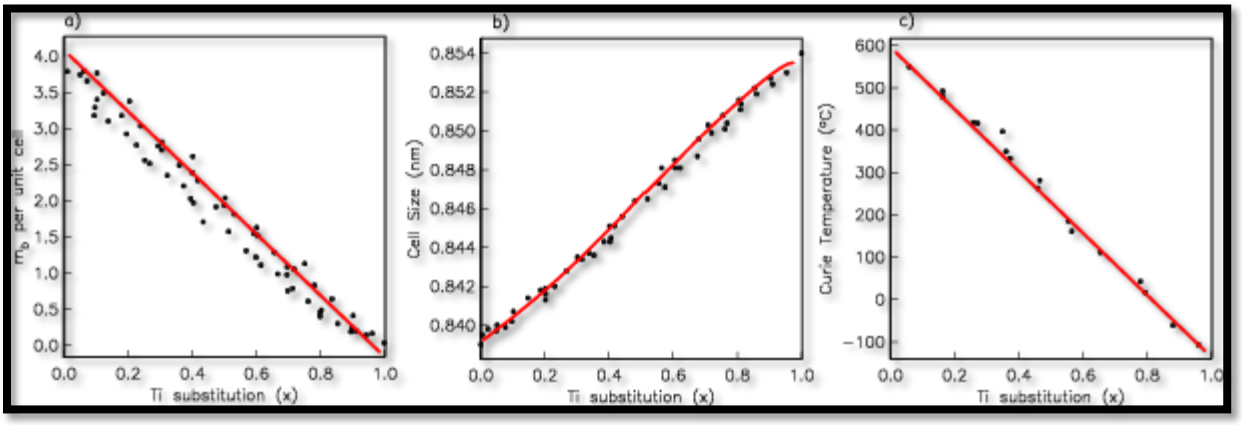

Figure 24. Relationships between Ti-Substitution and a) magnetization per unit cell, b) cell size, c) Curie temperature. (Dunlop 1986)

5.2 Methods

The Geofyzika KappaBridge at the IRM was used to collect high temperature susceptibility measurements. The appropriate samples were put in a glass test tube (Figure 5), and the tube was placed in the furnace apparatus as shown in Figure 18. The samples were heated up to 700 ˚C and then brought back to room temperature. The measurement increments varied as the temperature was increasing/decreasing.

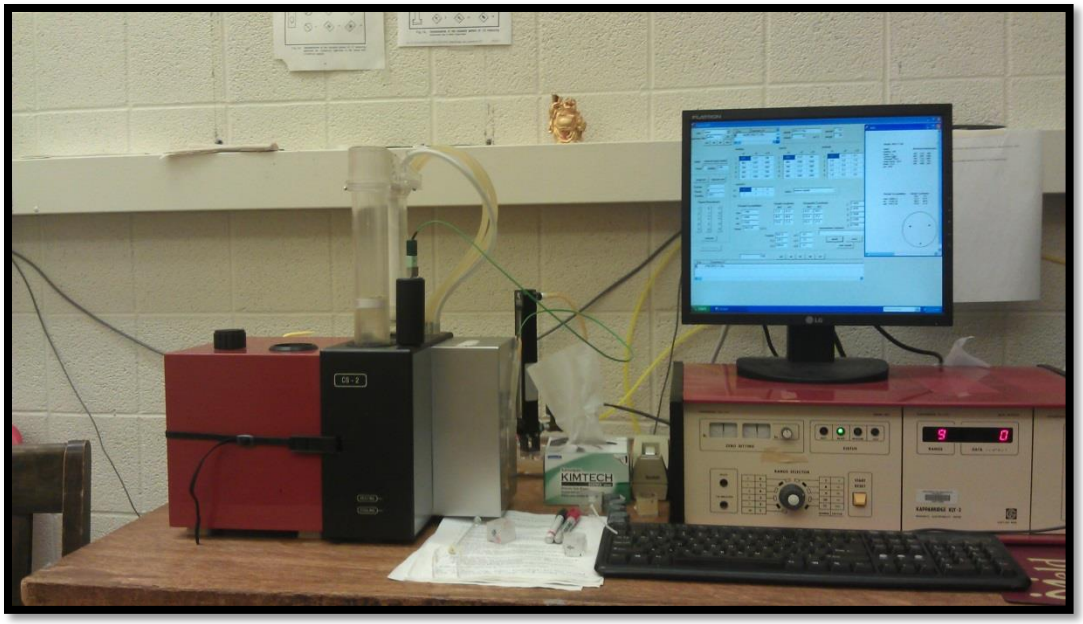

Figure 25. KappaBridge with high temperature setting.

5.3 Results

High temperature susceptibility results show a range of magnetic susceptibility from -2.86 to 12.52 m^3/kg (x 10^{-6}). Curie temperatures of all heating curves indicate some form of titanomagnetite in rocks of the BRD (Figures 26 and 27). The maximum titanium substitution (calculated from Curie temperatures using Dunlop et al 1986) was a value of 17%, as shown by the curie temperature of 455°C. Not all samples had reversible curves during cooling; this is an indication of alteration due to heating. Samples that had significant alteration showed evidence for the creation of TM40 with a curie point of 300°C during cooling. Most samples with alteration showed an increase in Ti-substitution as shown in Table 6 and in Figure 28 (refer to Appendix B for complete set of high temperature plots). Alternatively, a curie point of 300°C may indicate the presence of some sulfides such as Troilite, but the dominance of curie temperatures

between 575°C and 455°C suggests that Ti-poor titanomagnetite is the dominant magnetic mineral in BRD rocks.

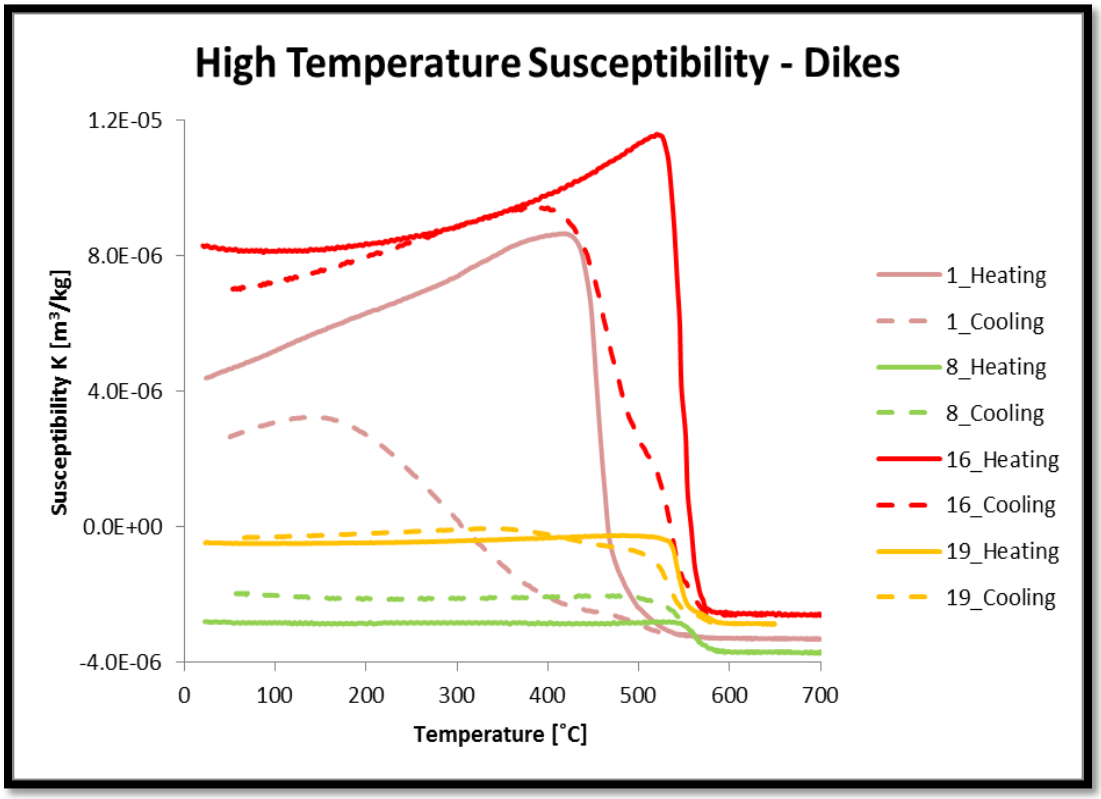

Figure 26. High Temperature susceptibility curves from dike sites.

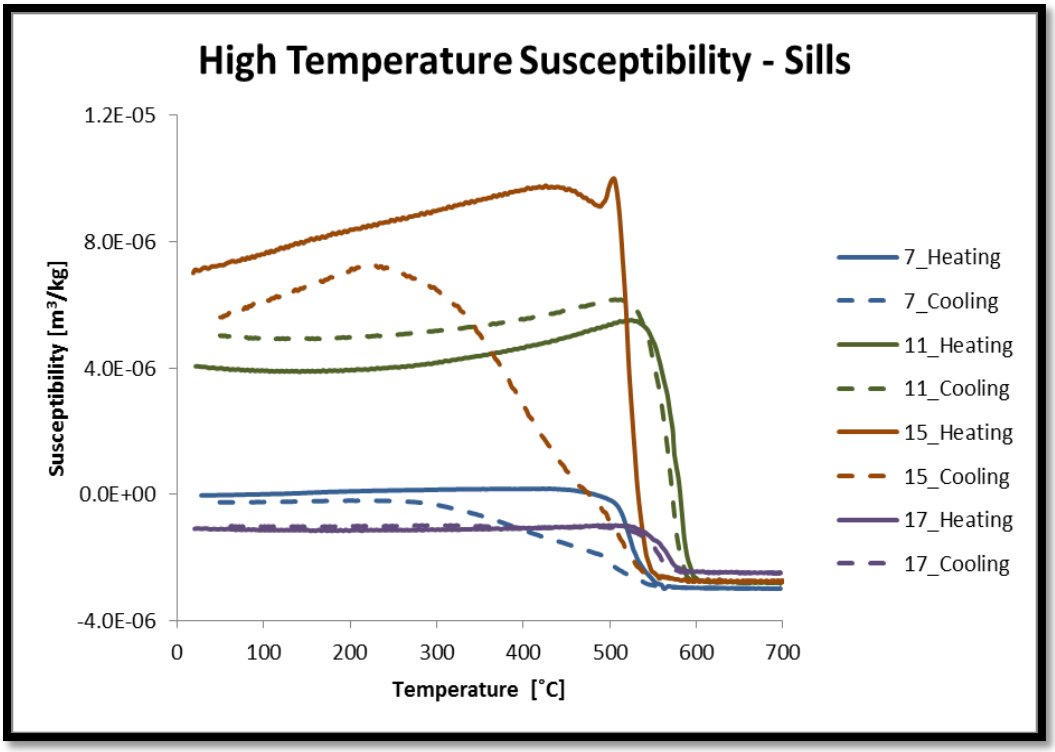

Figure 27. High Temperature Susceptibility Curves from Sill sites.

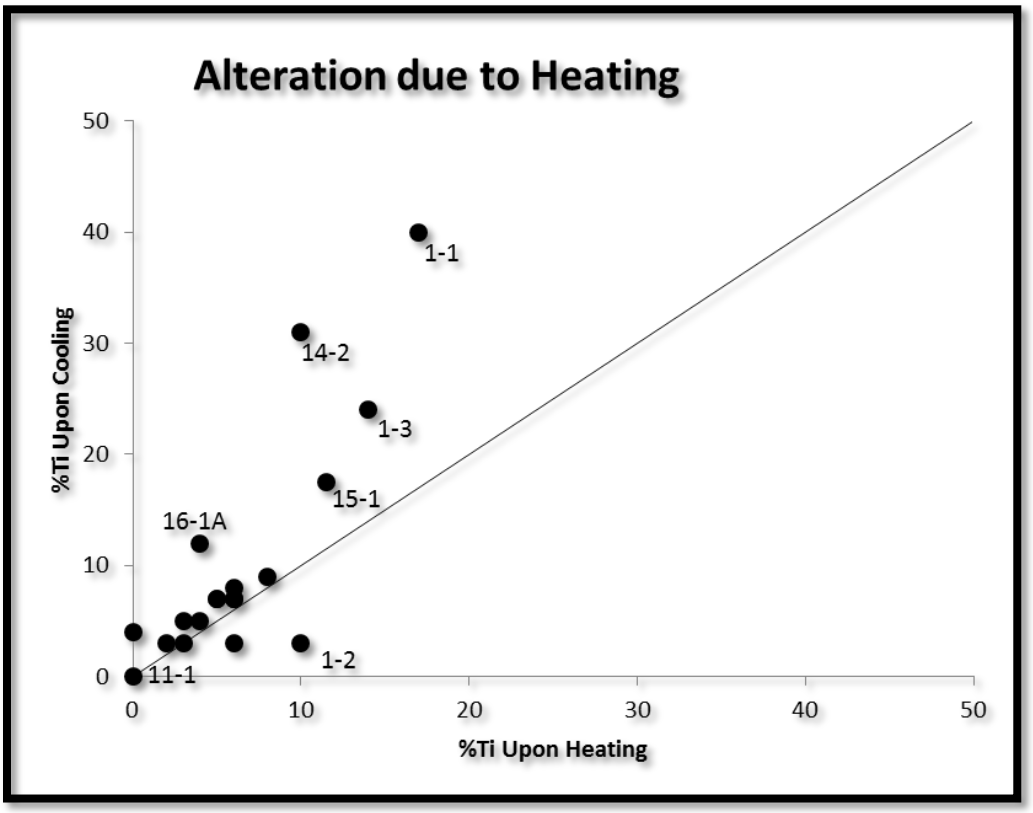

Figure 28. Alteration due to heating of BRD samples.

Table 6. High Temperature Susceptibility Data

Sample	Room Temp Susc. κ ($m^3/kg \times 10^{-6}$)	Reversible Curves	Curie Temp. (Heating) T_c (˚C)	Possible Magnetic Carrier (Heating)	Curie Temp. (Cooling) T_c (˚C)	Possible Magnetic Carrier (Cooling)
BRD-1-1	4.39	No	455	TM17	300	TM40 (Troilite?)
BRD-1-2	7.33	No	480/540	TM14/TM06	560	TM03
BRD-1-3	-0.22	No	480	TM14	410	TM24
BRD-2-1	12.52	Yes	542	TM05	533	TM07
BRD-3-1	4.30	Yes	515/560	TM09/TM03	488/555	TM13/TM03
BRD-4-1	-1.59	No	538/570	TM06/Magnetite	560	TM03
BRD-6-1	na	na	na	na	na	na
BRD-7-1	-0.04	No	523	TM08	503/533	TM11/TM07
BRD-8-1	-2.80	Yes	560	TM03 (Magnetite)	555	TM03
BRD-9-1	5.73	Yes	540	TM06	530	TM07
BRD-10-1	-1.91	No	570	Magnetite	550	TM04
BRD-11-1	4.05	Yes	577	Magnetite	568	Magnetite
BRD-12-1	0.49	Yes	550	TM04	545	TM05
BRD-13-1	-0.49	Yes	540	TM06	530	TM07
BRD-14-1	-2.86	Yes	555	TM03	545	TM05
BRD-14-2	3.61	No	510	TM10	360	TM31
BRD-15-1	7.00	No	470/523	TM15/TM08	390/513	TM26/TM09
BRD-16-1	8.30	No	550	TM04	460/530	TM17/TM07
BRD-17-1	-1.09	Yes	565	TM02 (Magnetite)	555	TM03
BRD-18-1	na	na	na	na	na	na
BRD-19-1	-0.47	No	543	TM05	530	TM07
BRD-20-1	na	na	na	na	na	na

Note: TMxx represents the percentage of Ti-substitution. Example: TM17 = 17% Ti-substitution.

5.4 Discussion

Alteration due to heating is evident in a few samples as indicated by irreversible curves. It is unclear why there is variation in the TM values, but for samples where alteration clearly occurred, the TM values increased during alteration as indicated by the lower Curie temperatures on cooling curves. Whether or not this observation provides any historical implication relating to the thermal conditions that were present during the crystallization of rocks from the BRD is unclear at the moment.

Furthermore, the amount of Ti substitution may be a result of proximity of specimens to the surface of the outcrop, as near surface specimens would be more subject to weathering and oxidation, and would be expected to have higher TM values compared with samples from deeper in the same core.

CHAPTER 6: SYNTHESIS OF RESULTS AND DISCUSSION

6.1 AMS Discussion

Some questions that can be asked with regards to the AMS data are as follows. Are minimum susceptibility axes perpendicular to flow direction in dikes and sills, and thus perpendicular to the plane of dikes and sills? The emplacement of dikes is normally vertical, and that of sills is usually horizontal. Does this mean that in dikes, the minimum susceptibility axes will be horizontal, and in sill the minimum susceptibility aces be vertical? If this is the case, then the samples can be grouped based on their minimum susceptibilities as indicators of whether the specimens came from dikes or sills.

It is known that magnetic fabric in igneous rocks may be formed by several geologic processes, including primary magma flow and deformation after emplacement (Ellwood, 1978, Hrouda, 1982, Tarling and Hrouda, 1993, Canon-Tapia, 2004, Zhang et al 2011). It has been established that the magnetic fabric of some igneous rocks is commonly related to their emplacement mechanism and the magmatic flow directions can be reconstructed from the orientation of the magnetic ellipsoids. This is what makes AMS a useful technique to infer magma flow direction and source. AMS can also provide clues concerning the extent of deformation.

In rocks where magnetic susceptibility is carried by ferrimagnetic minerals like titanomagnetite or magnetite, the origin of the AMS is related to the grain shape (shape anisotropy). In this case, k1 is parallel to the long axis of the particle (for multi-domain) and pseudo-single domain grains.

To correctly interpret the direction of the maximum and minimum susceptibility axes, the fabrics have to be determined. There are three types of fabrics, “normal”,

“intermediate”, and “inverse” (Rochette et al 1991, 1992). These fabrics are defined by considering the relationship between the dike plane and the AMS eigenvectors. Normal fabric happens when the AMS foliation (K1-K2) plane is nearly parallel to the dike plane and magnetic foliation pole (K3) is nearly perpendicular to it. Intermediate fabric happens when K1 and K3 cluster close to the dike plane, while K2 is nearly perpendicular to this plane. Inverse fabric occurs when K2 and K3 form a plane parallel to the dike plane, and K1 is perpendicular to the dike wall. Most of the time however, measurements yield a random or disturbed distribution of these three axes, as was the case in this study. In general, normal fabrics are expected in the middle of dikes or sills, and intermediate and inverse fabrics are expected near the chilled margins.

Although magnetic lineation K1, is generally assumed to be flow related, it turns out that it is not always a reliable flow direction indicator. K1 can be flow perpendicular and parallel in lava flows in dikes, and sometimes completely unrelated to flow direction (Geoffroy et al 2002, Gil-Imaz et al 2006). For normal fabrics, it is established that k1 approximates the maximum stretching axis of a finite ellipsoid and k3 parallels to the maximum shortening axes (Hrouda 1982).

Types of fabrics need to be defined in rocks to determine flow. Since there was no contact data available in the field, the type of fabric can’t be determined with certainty (whether it is normal, or inverse). Thus, making flow direction and fabric conclusions from the AMS results obtained in this study are difficult.

6.2 Hysteresis Loops, High Temperature Susceptibility and Grain Size

While the relationship between grain size and hysteresis parameters have been shown in several studies, it is difficult to know for certain the reasons behind the

saturation magnetization and coercivity values. Is the saturation magnetization a result of the percentage of magnetic minerals in a sample, or is it the result of the grain size and thus the domain state of the mineral? Is it a combination of both? In the presence of exsolution, it has been shown that titanium substitution decreases the grain size available for magnetic moments to align within. This in turn changes the domain state of a mineral from MD or PSD to SD since the smaller the grain size, the more likely it will be SD.

The low values of titanium substitution in the BRD then suggests that the grain size is such that PSD states are possible, as indicated by the Day plot (Figure 21). Specimens with higher titanium substitution can then be considered to have higher exsolution levels, which in turn mean they would have higher Mr/Ms ratios, and lower Hcr/Hc ratios.

6.3 Excluded Samples

It should be noted that not all samples were included as part of this study. Site 5-1 was not a BRD outcrop, the sample extracted was anorthosite. Due to time constraints, not all specimens were measured across all the experiments performed.

6.4 Possible Future Work

Future analysis will investigate the relationship of AMS to rock fabric by measuring mineral crystal preferred orientations using electron backscatter diffraction. These measurements will supplement the AMS data, and provide links to the role of microstructure, texture and mineralogy in AMS. In addition, petrologic and microscope imagine of grains will help in determining grain size and mineralogy and comparing it to the results obtained from this study.

CHAPTER 7 – CONCLUSION

The hypotheses of this study were:

1. The magnetic mineralogy in the BRD should be due to magnetite or some variant composition.
2. If the BRD was emplaced through a main feeder dike arc oriented NE-SW, then flow directions in subsequent sills and dikes should be away from the feeder dike, or in SE-NW orientations.

Hysteresis properties and high temperature susceptibility measurements indicate a PSD composition of titanomagnetite with a range of Ti-substitution ratios between zero and 17%, and with a grain size between 0.1 and 20 microns to be the dominant magnetic carrier of rocks from the BRD.

No measurements of contacts were made in the field with regards to the outcrops sampled in this study, thus conclusions regarding dikes and sills in terms of AMS cannot be made with confidence. Given that the magnetic fabrics in both dikes and sills can be inverted near the chilled margins, and since we were unable to determine proximity to chilled margin in the field due to poor outcrop coverage, we cannot assume that Kmax is perpendicular to dike or sill walls. The bootstrap stereonet projections indicate support for NW-SE flow directions in dikes and sills away from the feeder dike. The AMS results show that most samples are triaxial with relatively low anisotropy values. Some samples, however do exhibit high anisotropy and shape factors that are oblate, which is consistent with settling or compaction.

APPENDIX A – DATA TABLES

Table A1. General Properties of Specimens collected from each site.

Specimen_ID	Specimen_azimuth	Specimen_plunge	Specimen_mass[g]	Notes
BRD-1-1Aa	340	68.5	32.0767	
BRD-1-1Ba	340	58	31.1775	
BRD-1-1Ca	320.5	63	30.1396	
BRD-1-1Da	339	64.5	31.1241	
BRD-1-1Ea	306	71	31.8565	
BRD-1-1Fa	295	73.5	31.7652	B
BRD-1-1Ga	337.5	64	31.613	B
BRD-1-2Aa	300	65.5	28.8327	
BRD-1-2Ba	290	44.5	31.5904	
BRD-1-2Ca	286.5	54	30.1841	
BRD-1-2Da	326.5	69	26.5585	Short
BRD-1-2Ea	290.5	60	30.5953	
BRD-1-3Aa	303	47	31.8359	
BRD-1-3Ba	302	59.5	31.7296	
BRD-1-3Ca	306	52	31.6292	
BRD-1-3Da	320	73.5	29.9551	
BRD-1-3Ea	318	85	28.7742	
BRD-2-1Aa	307	71	31.1954	
BRD-2-1Ba	323	78	31.4046	
BRD-2-1Ca	270	81.5	32.1207	
BRD-2-1Da	311	72	31.4165	B
BRD-2-1Ea	259.5	91.5	32.6549	
BRD-2-1Fa	293	77.5	28.3894	
BRD-3-1Aa	55	74	26.3711	O
BRD-3-1Ba	285	85	30.0812	Scr
BRD-3-1Ca	349.5	99	7.61802	O
BRD-3-1Da	0	68	31.3956	O
BRD-3-1Ea	20	75.5	29.3831	O
BRD-3-2Aa	358	52.5	30.5133	
BRD-3-2Ba	278	87.5	26.2674	
BRD-3-2Ca	350	81.5	27.4338	
BRD-4-1Aa	308.5	54.5	30.755	HdTh
BRD-4-1Ba	288	97.5	31.264	HdTh
BRD-4-1Ca	286	11.5	30.5444	HdTh
BRD-4-1Da	285	42.5	31.2197	B/HdTh
BRD-4-1Ea	297	80.5	31.5419	B/HdTh
BRD-5-1Aa	172	89.5	25.7698	Anthrst

BRD-6-1Aa	341	70	28.3683	
BRD-7-1Aa	277.5	98	28.4439	Slmp
BRD-7-1Ba	287	97	28.473	Slmp
BRD-7-1Ca	5	92	32.2225	Slmp
BRD-7-1Da	240	75.5	28.9083	Slmp
BRD-7-1Ea	295	91	26.9211	Slmp
BRD-7-1Fa	298	95	28.8474	Slmp
BRD-8-1Aa	282	89	24.9814	B
BRD-8-1Ba	332	56	27.8302	
BRD-8-1Ca	294	65	30.4849	
BRD-8-1Da	303.5	66	25.7512	B
BRD-8-1Ea	306	90.5	26.0493	B
BRD-8-1Fa	285	82.5	26.7155	B/P
BRD-9-1Aa	292	77	30.7074	B
BRD-9-1Ba	307.5	87	30.8513	B
BRD-9-1Ca	310	84	30.2908	
BRD-9-1Da	310	67	31.4745	
BRD-10-1Aa	107	73	31.0093	B
BRD-10-1Ba	100	74	30.4264	
BRD-10-1Ca	100	93.5	31.2987	
BRD-10-1Da	100	89.5	30.7677	
BRD-10-1Ea	100	89	30.7933	
BRD-10-1Fa	100	79.5	31.0999	
BRD-11-1Aa	138	75.5	26.545	
BRD-11-1Ba	131	84	27.35	
BRD-11-1Ca	109	64	30.0692	
BRD-11-1Da	59	93.5	29.7199	B
BRD-11-1Ea	17	92	28.4545	
BRD-11-1Fa	345.5	48.5	31.2837	
BRD-11-1Ga	21	36	31.2058	B/P
BRD-12-1Aa	359	58	32.2499	
BRD-12-1Ba	0	56	32.3646	
BRD-12-1Ca	160	45	32.284	B
BRD-12-1Da	171	36	32.1814	
BRD-12-1Ea	178	78.5	32.003	
BRD-12-2Aa	124	74	28.3415	
BRD-12-2Ba	164	83.5	32.0488	
BRD-12-2Ca	133	79	29.5394	B
BRD-12-2Da	134	76	31.5862	
BRD-12-2Ea	90	84.5	31.5366	B

BRD-12-2Fa	158	73.5	32.1564	
BRD-12-2Ha	11	80	29.9593	
BRD-13-1Aa	272	82	26.6849	
BRD-13-1Ba	299	72	31.8231	
BRD-13-1Ca	285	83.5	31.2022	
BRD-13-1Da	314	85.5	28.4974	
BRD-13-1Ea	297	66	31.9678	
BRD-13-1Ga	297	65.5	28.9677	
BRD-14-1Aa	241	55	32.3592	O
BRD-14-1Ba	232	63.5	32.3592	O
BRD-14-1Ca	254.5	54	28.912	O
BRD-14-1Da	262	45	32.4276	O
BRD-14-1Ea	260	85	32.2238	O
BRD-14-1Fa	266	54	32.2606	O
BRD-14-2Aa	263.5	83	31.875	
BRD-14-2Ba	173	40.5	31.9695	B
BRD-14-2Ca	189	47.5	30.7271	B
BRD-14-2Da	206	81	33.0767	
BRD-14-2Fa	203	82	29.5023	
BRD-14-2Ga	225	70	32.0438	
BRD-14-2Ha	287	49	28.088	
BRD-15-1-Da	341	51.5	27.5262	
BRD-15-1-Ea	345	67	29.3066	
BRD-15-1Aa	229.5	70.5	27.7916	
BRD-15-1Ba	331.5	63	29.1058	
BRD-15-1Ca	339	60.5	28.0529	
BRD-16-1Aa	337	84	27.4736	MA
BRD-16-1Ba	338	76	30.3596	MA
BRD-16-1Ca	275	84	31.5184	MA
BRD-16-1Da	345	92	27.3779	MA
BRD-16-1Ea	7	87	31.0281	MA
BRD-16-1Fa	201	90	28.9325	MA
BRD-17-1Aa	176	79.5	31.8144	
BRD-17-1Ba	195	76	28.5729	
BRD-17-1Ca	62	57.5	29.7183	
BRD-17-1Da	102	47	30.5658	
BRD-17-1Ea	173.5	36	28.8608	
BRD-17-1Fa	271	33	32.2854	
BRD-18-1Ba	305	87	28.5105	
BRD-18-1Ca	355.5	88.5	28.1742	

BRD-18-1Da	12	39	32.3209	
BRD-18-1Ea	299	55.5	32.4174	
BRD-18-1Fa	308	46	32.7792	
BRD-19-1Aa	275	74	32.2786	W
BRD-19-1Ba	350	40.5	30.6492	W
BRD-19-1Ca	2	45	28.4715	W
BRD-19-1Da	276	78	33.0824	W
BRD-19-1Ea	14	45.5	32.6548	W
BRD-19-1Fa	274	78.5	29.9566	W
BRD-19-1Ga	275	79.5	26.6996	W
BRD-20-1Aa	279	86	31.1695	
BRD-20-1Ba	315	94.5	30.1963	
BRD-20-1Da	191	19	26.9578	
BRD-20-1Ea	270	90	32.3237	
BRD-20-1Fa	275	46	31.3311	B

B	Broken
O	Outcrop Possibly out of Place
HdTh	Possible Hydrothermal Alteration
Antrhst	Anorthosite
Slmp	Possibly Slumping
B/P	Broken/Poorly Oriented
Scr	Oriented from a Scratch not Copper
MA	Magnetic Anamoly affecting compass
W	Possibly weathered

APPENDIX B – ADDITIONAL PLOTS AND FIGURES

Category A – Low Magnetization, Small Grain Size, Low Coercivity

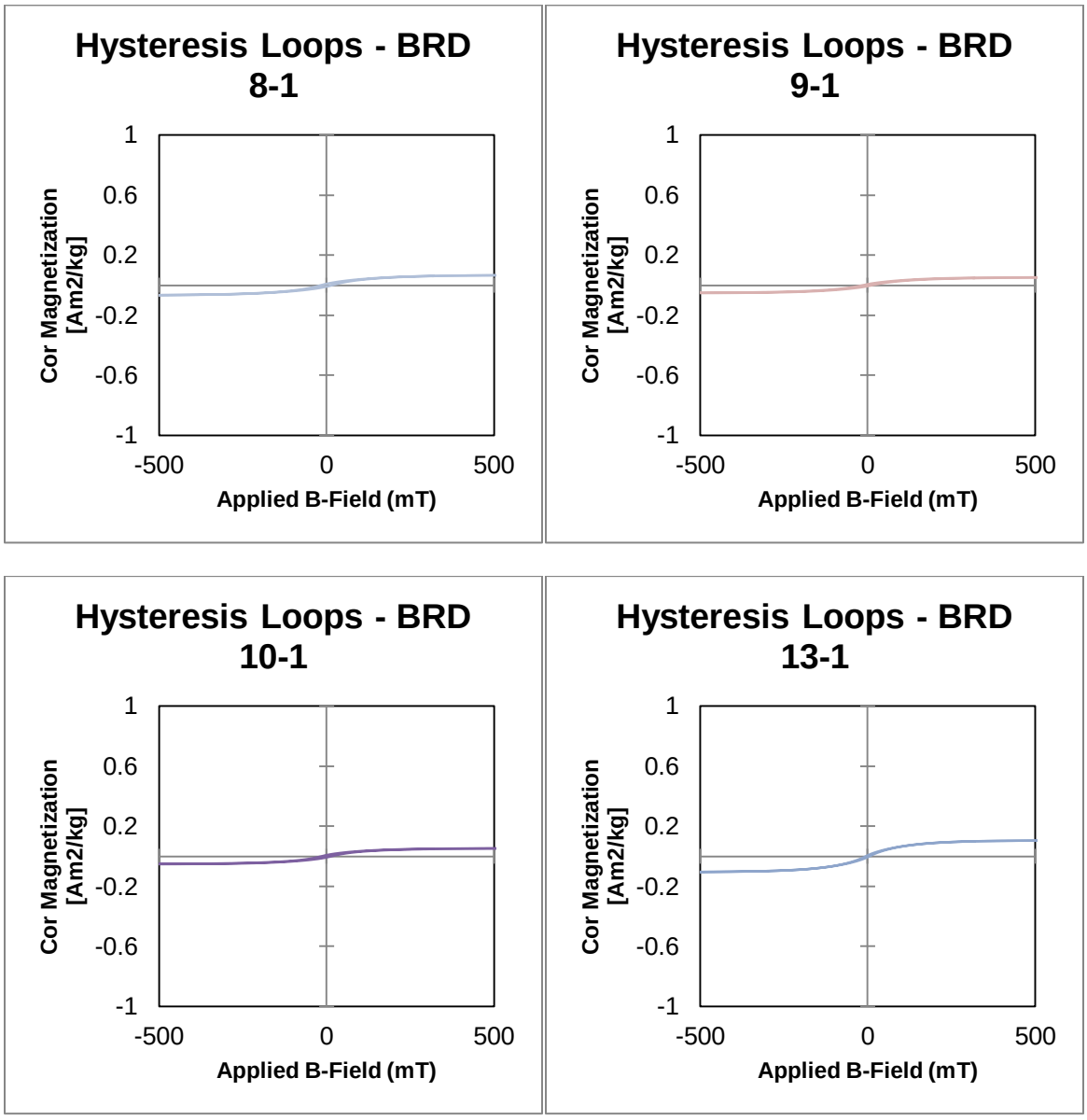

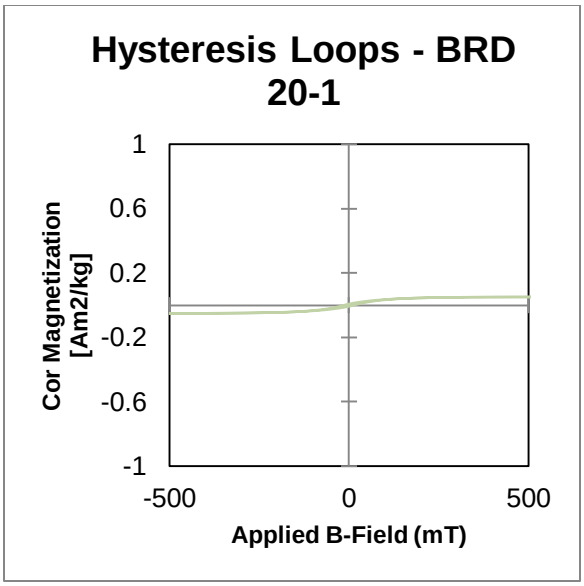
Hysteresis Loops - BRD 20-1
Cor Magnetization [Am2/kg]
1
0.6
0.2
-0.2
-0.6
-1
-500
0
500
Applied B-Field (mT)

Category B – Low Magnetization, Small Grain Size, Medium Coercivity

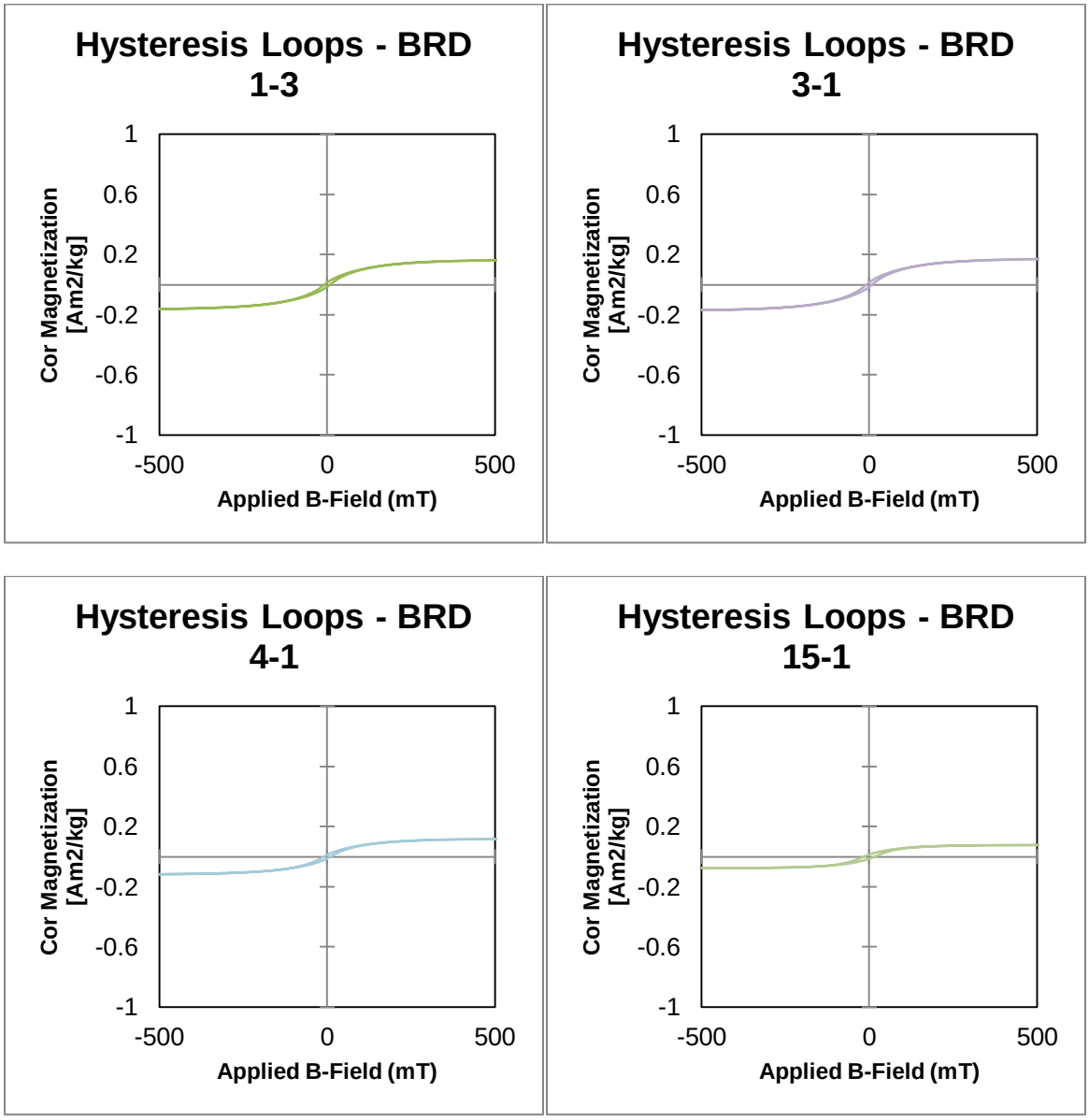

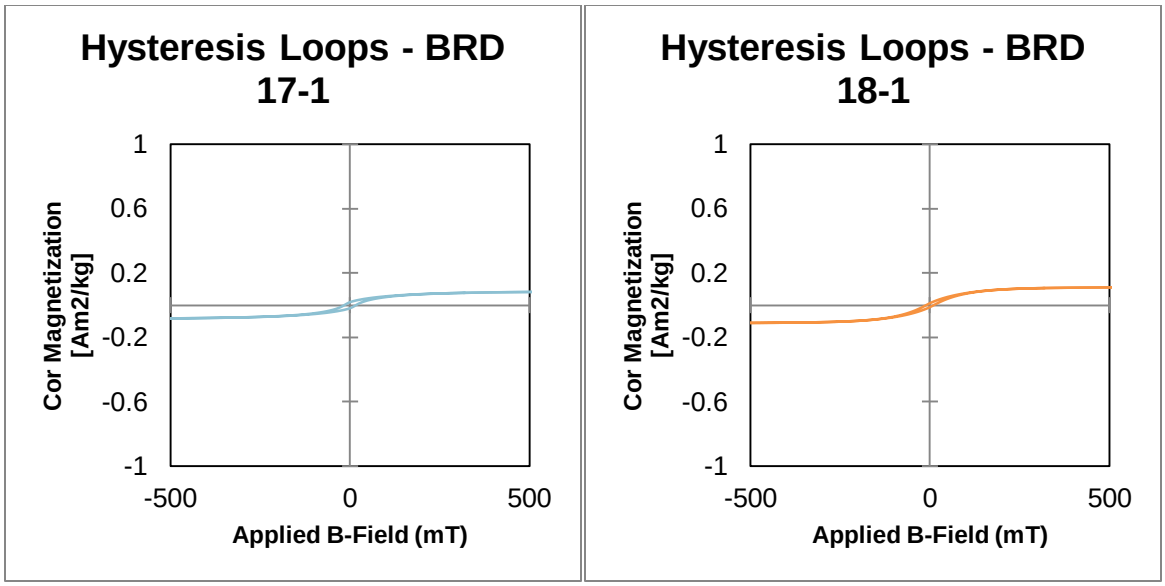
Hysteresis Loops - BRD 17-1
Cor Magnetization [Am2/kg]
1
0.6
0.2
-0.2
-0.6
-1
-500
0
500
Applied B-Field (mT)
Hysteresis Loops - BRD 18-1
Cor Magnetization [Am2/kg]
1
0.6
0.2
-0.2
-0.6
-1
-500
0
500
Applied B-Field (mT)

Category C – Low magnetization, higher coercivity, small grain size

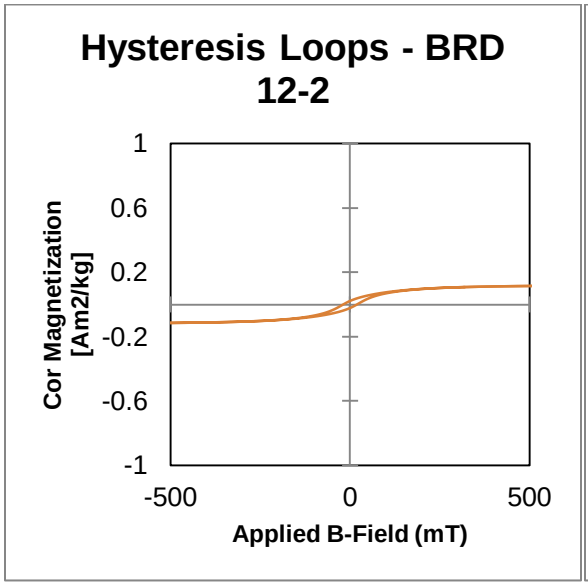

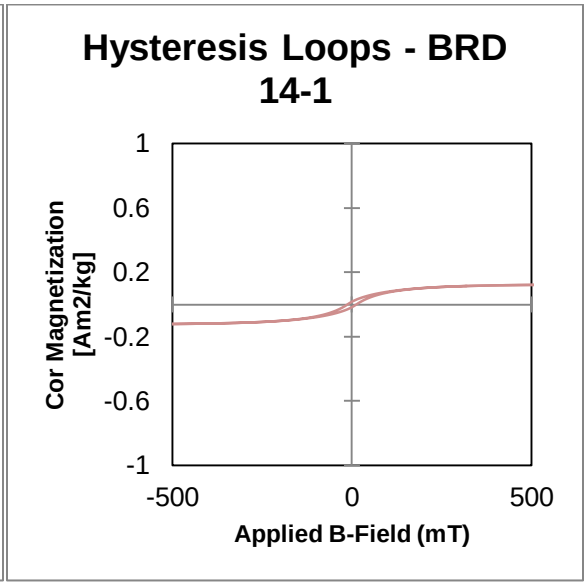

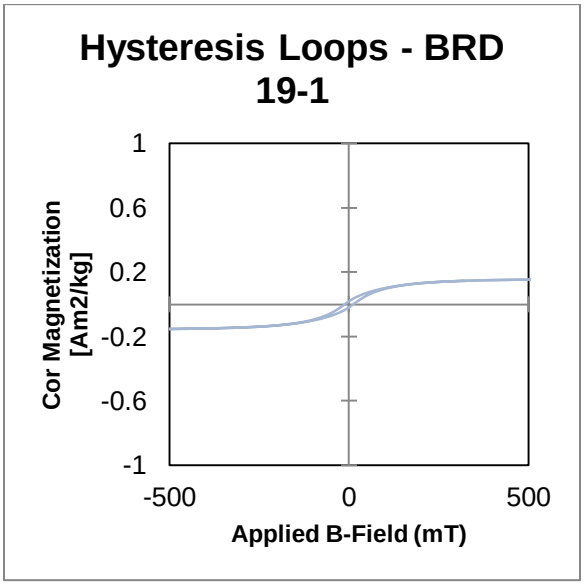

Category D – Intermediate Magnetization, Varying Coercivity, Medium Grain Size

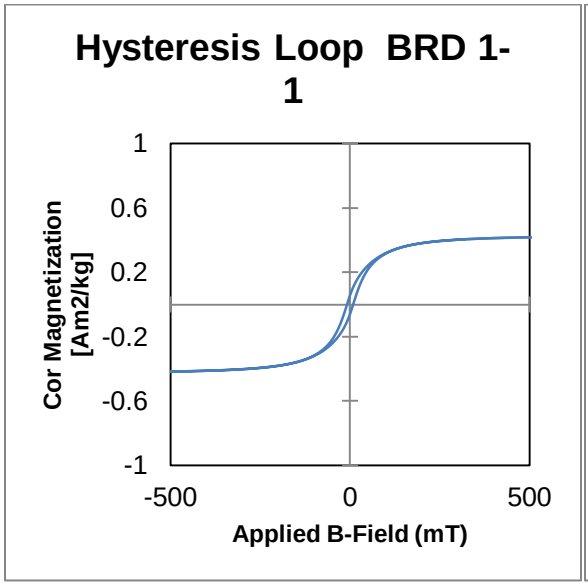

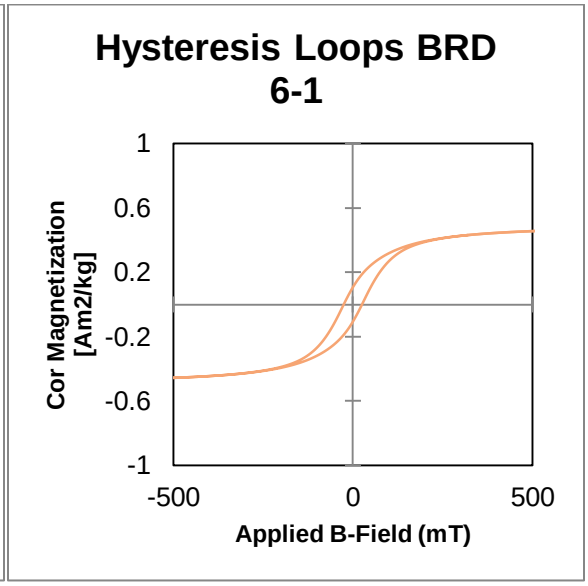

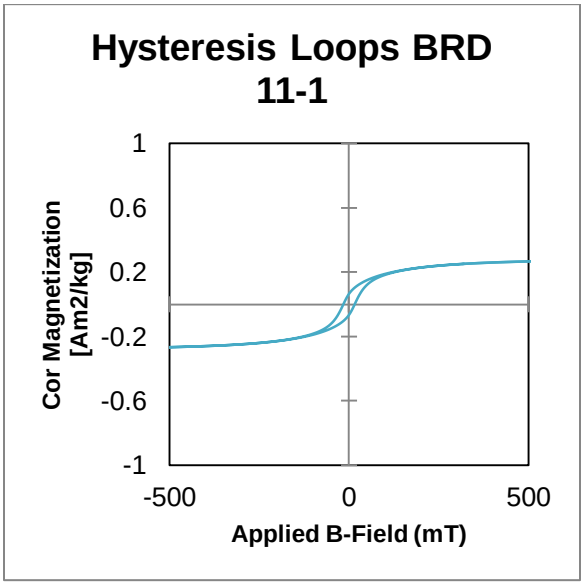

Category E – High Magnetization, Large Grain Size, varying coercivity

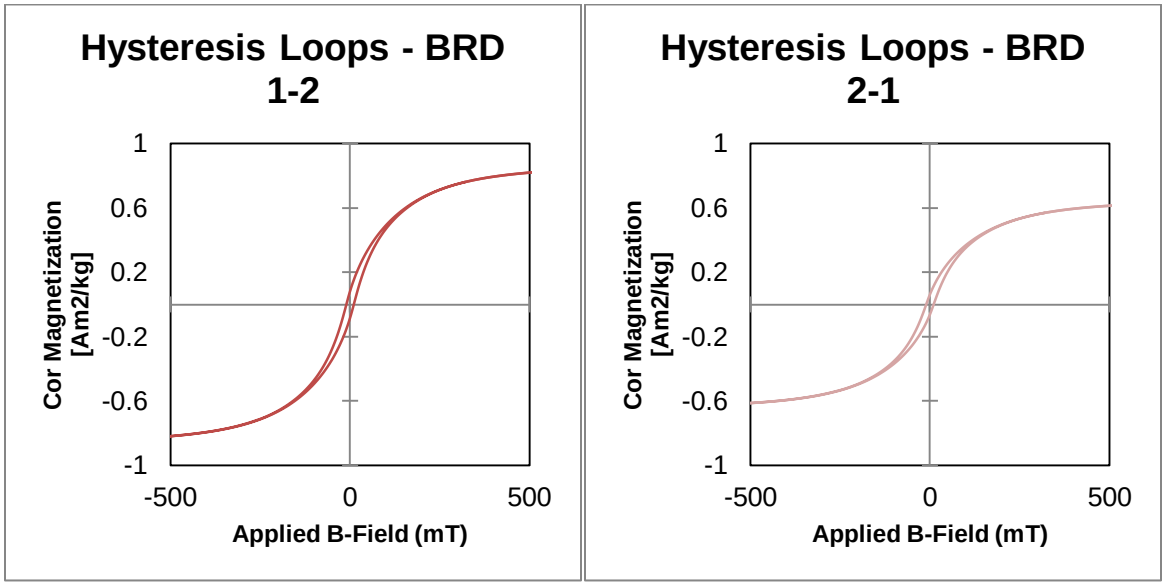

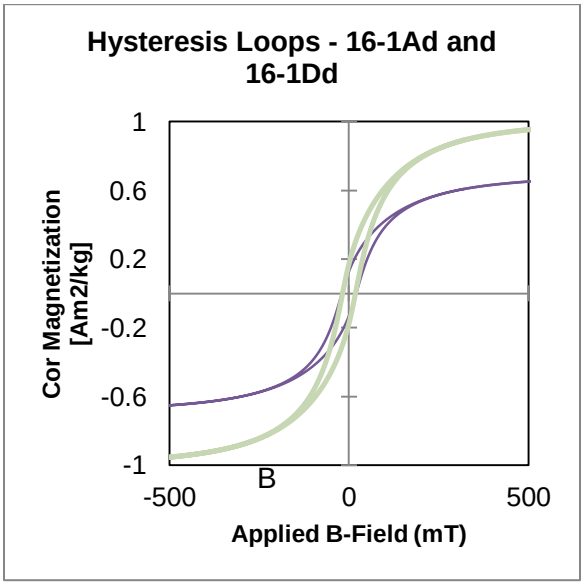

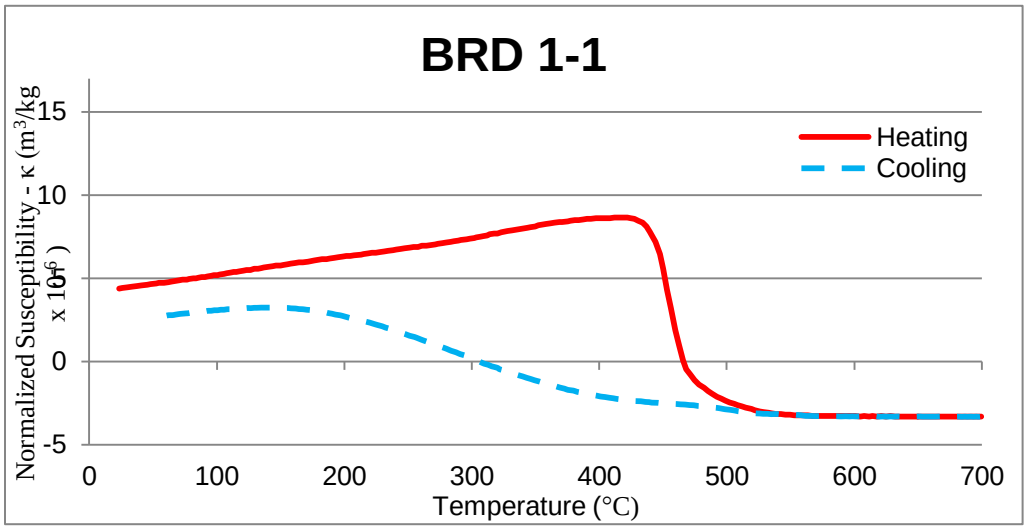
BRD 1-1
Normalized Susceptibility - κ (m3/kg x 10-6)
15
10
5
0
-5
0
100
200
300
400
500
600
700
Temperature (°C)
Heating
Cooling

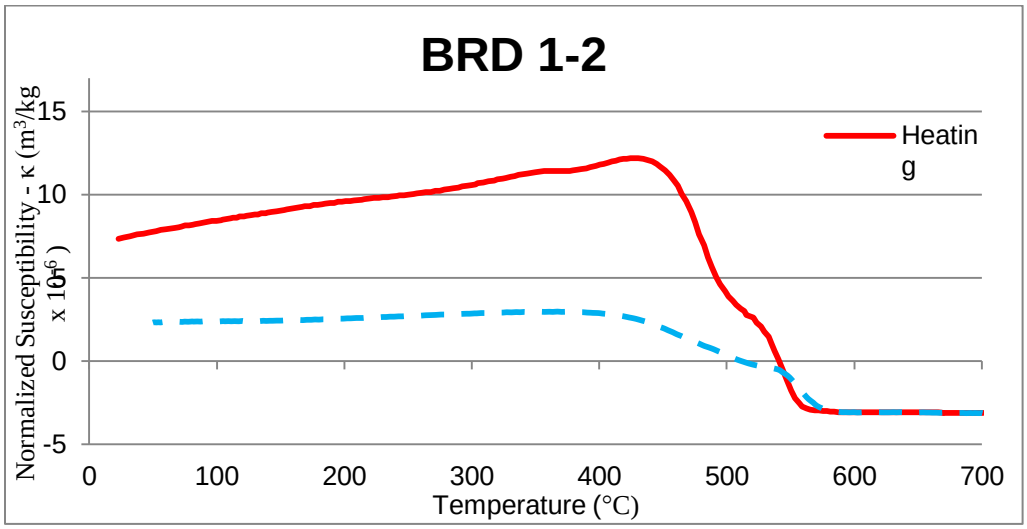
BRD 1-2
Normalized Susceptibility - κ (m3/kg x 10-6)
15
10
5
0
-5
0
100
200
300
400
500
600
700
Temperature (°C)
Heatin
g

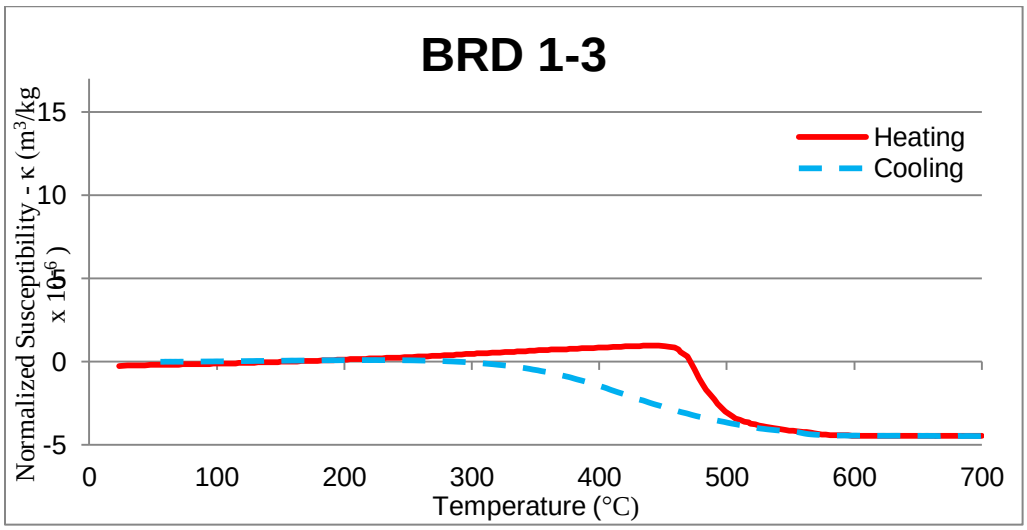
BRD 1-3
Normalized Susceptibility - κ (m3/kg x 10-6)
15
10
5
0
-5
0
100
200
300
400
500
600
700
Temperature (°C)
Heating
Cooling

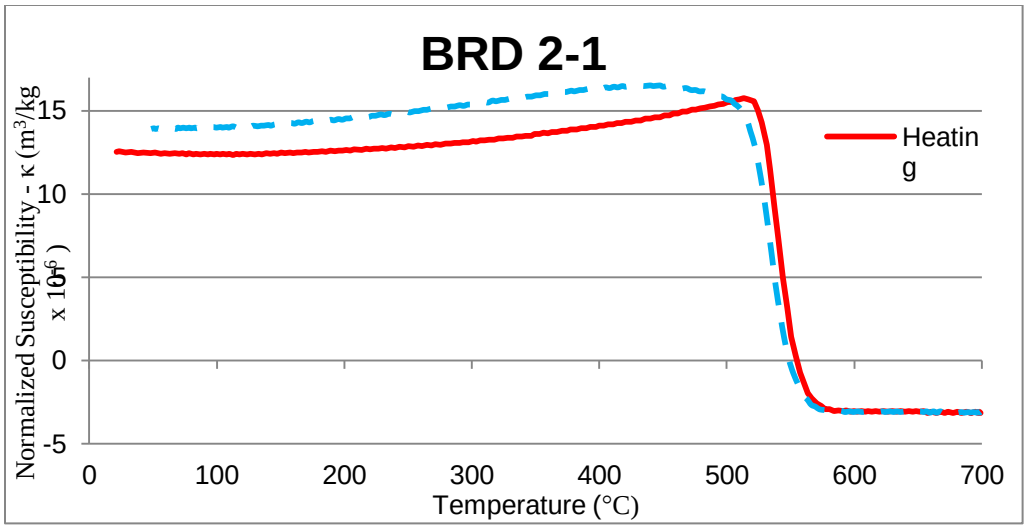
BRD 2-1
Normalized Susceptibility - κ (m³/kg x 10⁻⁶)
15
10
0
-5
0
100
200
300
400
500
600
700
Temperature (°C)
Heatin
g

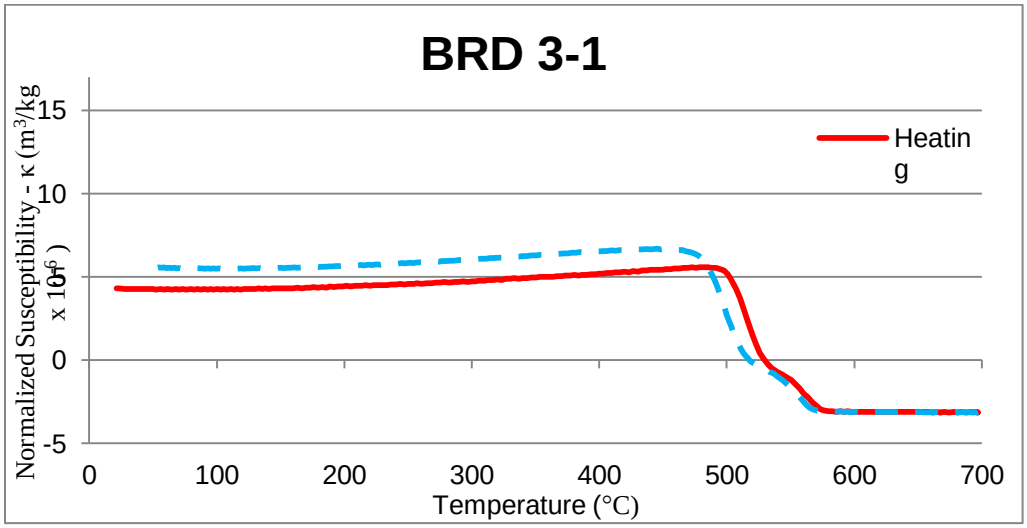
BRD 3-1
Normalized Susceptibility - κ (m³/kg x 10⁻⁶)
15
10
0
-5
0
100
200
300
400
500
600
700
Temperature (°C)
Heatin
g

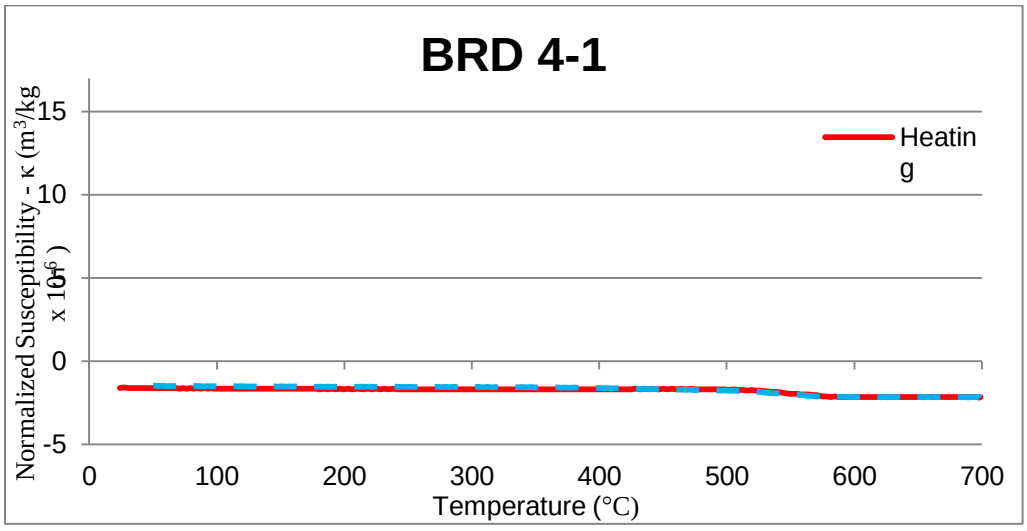
BRD 4-1
Normalized Susceptibility - κ (m³/kg x 10⁻⁶)
15
10
0
-5
0
100
200
300
400
500
600
700
Temperature (°C)
Heatin
g

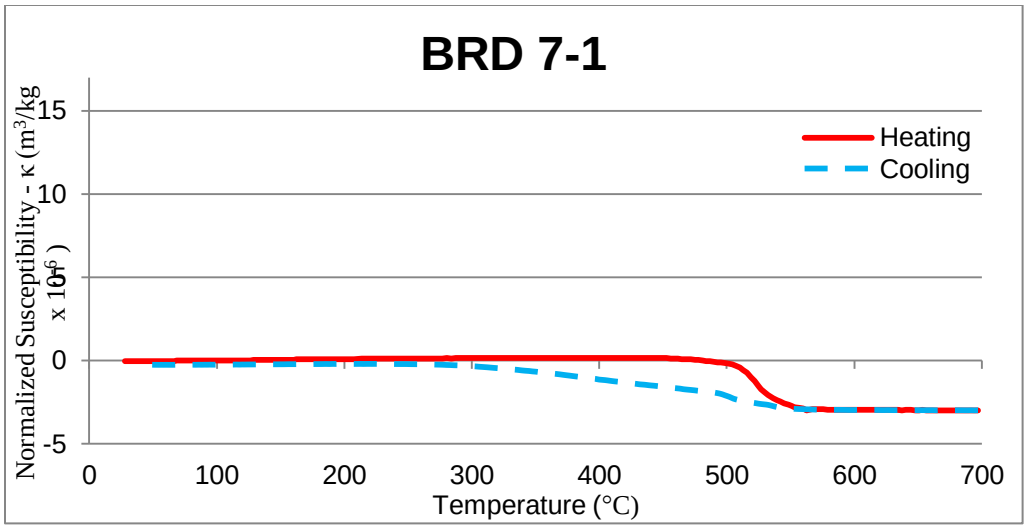
BRD 7-1
Normalized Susceptibility - κ (m3/kg x 10-6)
15
10
0
-5
0
100
200
300
400
500
600
700
Temperature (°C)
Heating
Cooling

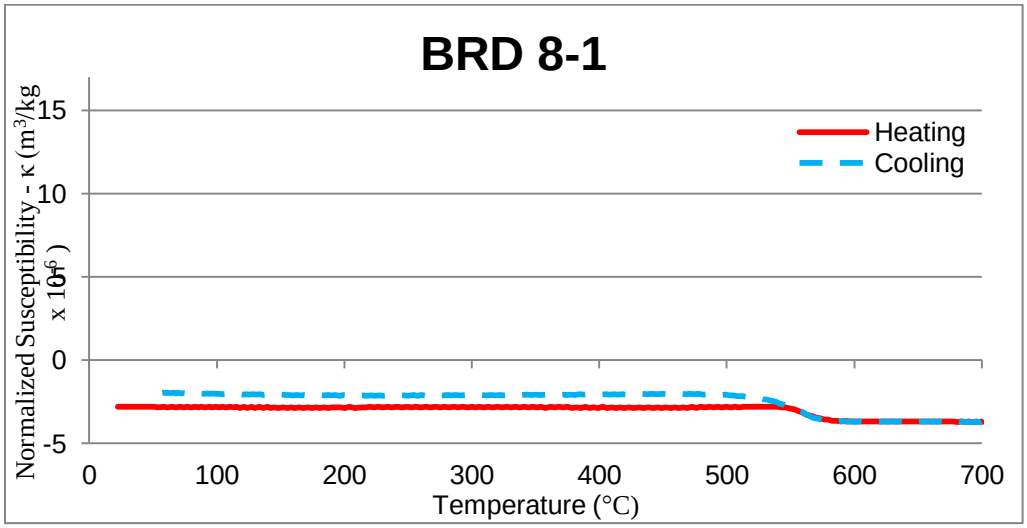
BRD 8-1
Normalized Susceptibility - κ (m3/kg x 10-6)
15
10
0
-5
0
100
200
300
400
500
600
700
Temperature (°C)
Heating
Cooling

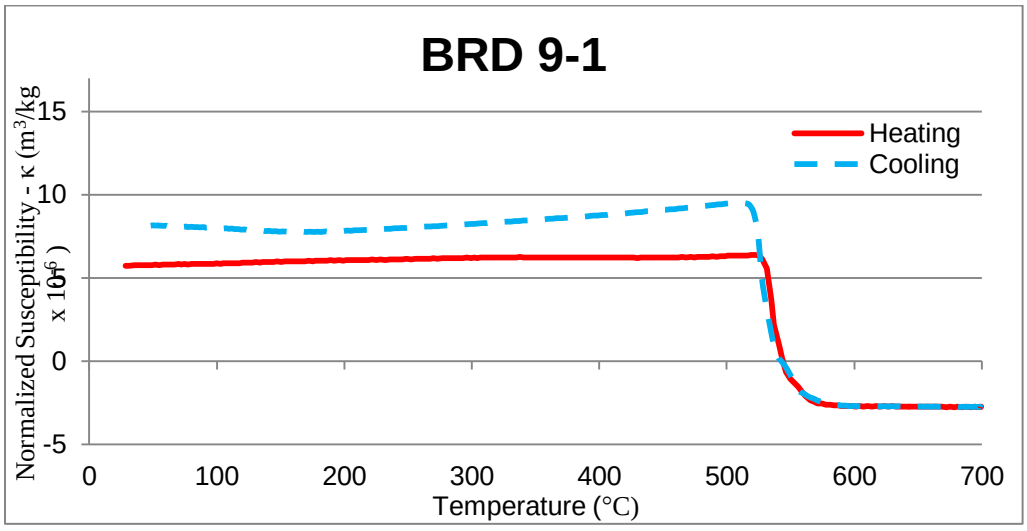
BRD 9-1
Normalized Susceptibility - κ (m3/kg x 10-6)
15
10
0
-5
0
100
200
300
400
500
600
700
Temperature (°C)
Heating
Cooling

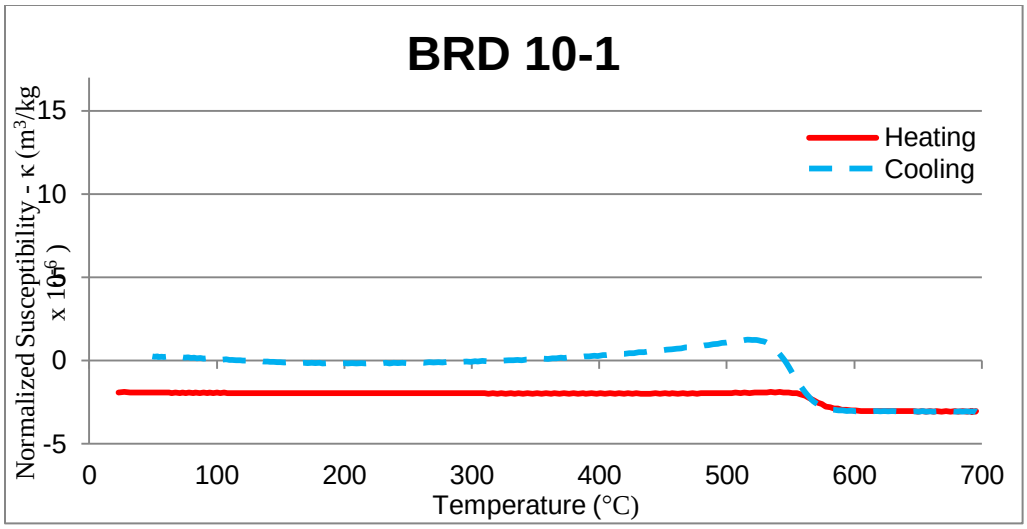
BRD 10-1
Normalized Susceptibility - κ (m3/kg x 10-6)
15
10
0
-5
0
100
200
300
400
500
600
700
Temperature (°C)
Heating
Cooling

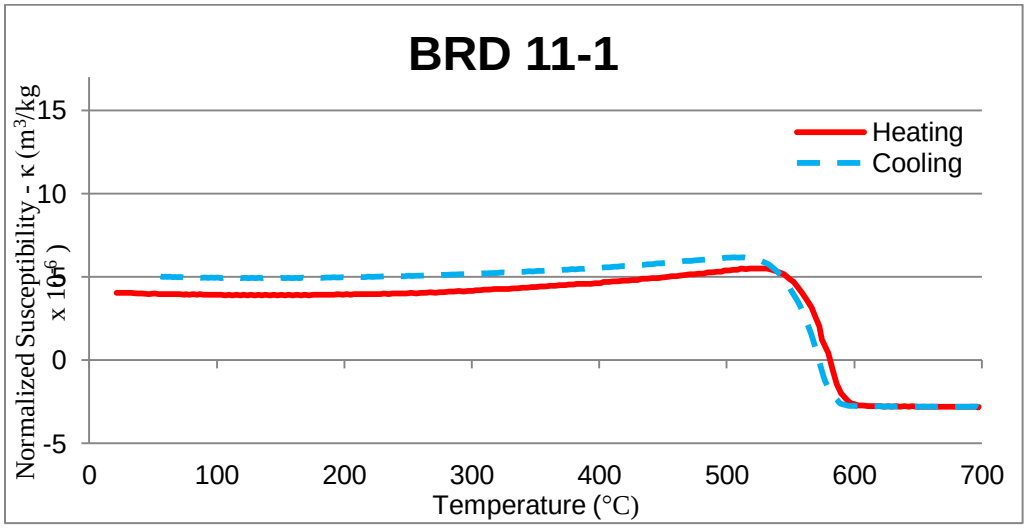
BRD 11-1
Normalized Susceptibility - κ (m3/kg x 10-6)
15
10
0
-5
0
100
200
300
400
500
600
700
Temperature (°C)
Heating
Cooling

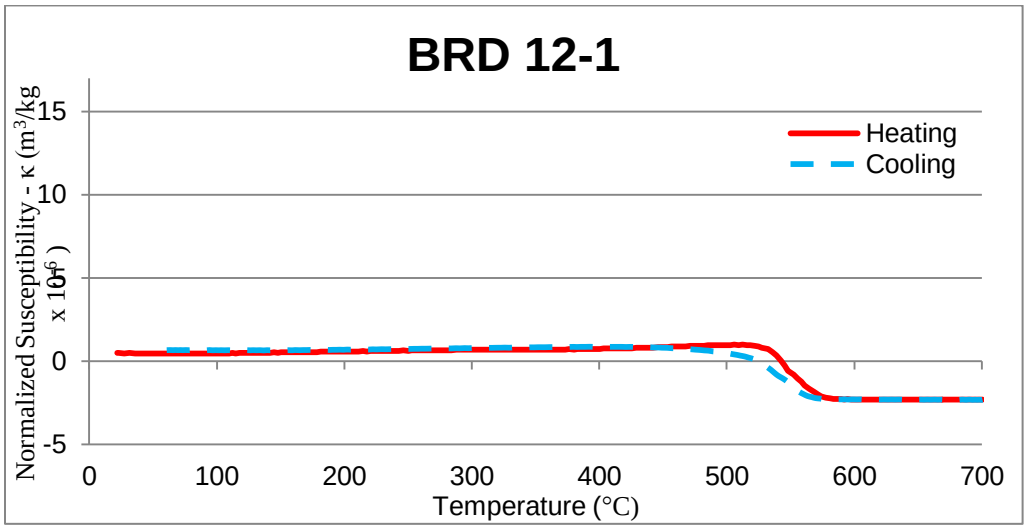
BRD 12-1
Normalized Susceptibility - κ (m3/kg x 10-6)
15
10
0
-5
0
100
200
300
400
500
600
700
Temperature (°C)
Heating
Cooling

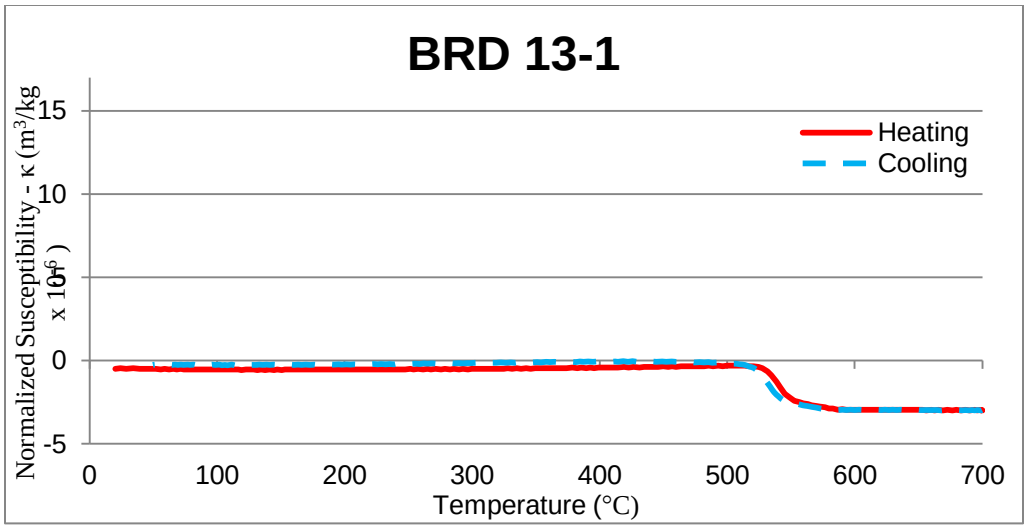
BRD 13-1
Normalized Susceptibility - κ (m3/kg x 10-6)
15
10
0
-5
0
100
200
300
400
500
600
700
Temperature (°C)
Heating
Cooling

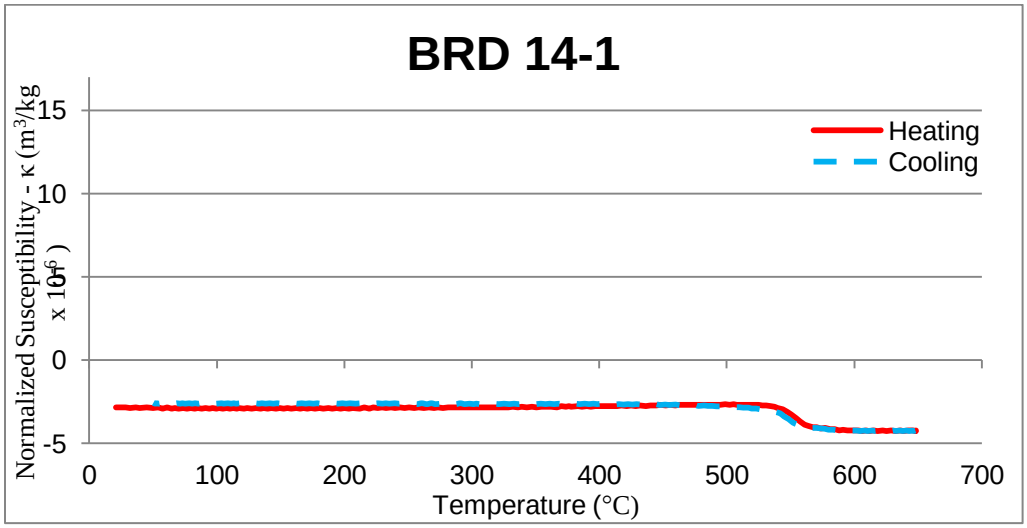
BRD 14-1
Normalized Susceptibility - κ (m3/kg x 10-6)
15
10
0
-5
0
100
200
300
400
500
600
700
Temperature (°C)
Heating
Cooling

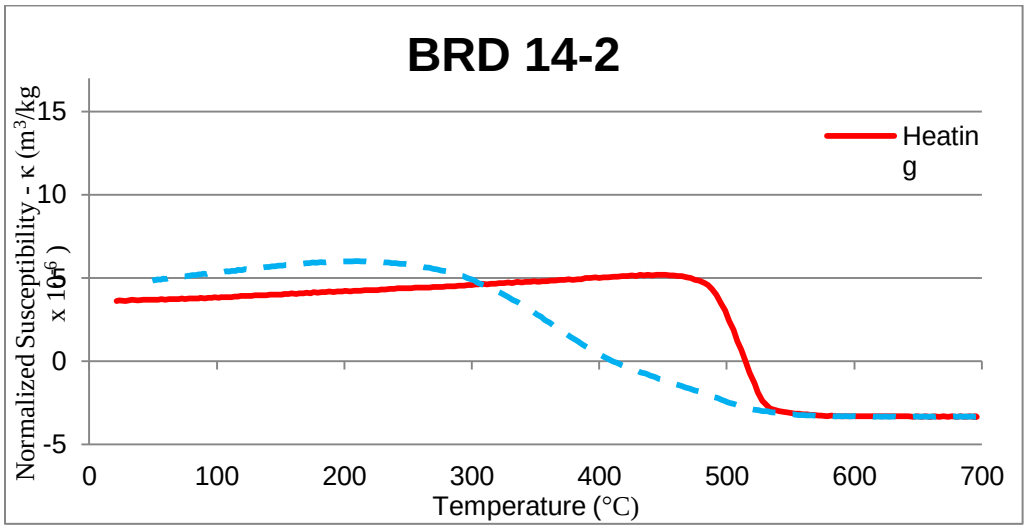
BRD 14-2
Normalized Susceptibility - κ (m3/kg x 10-6)
15
10
0
-5
0
100
200
300
400
500
600
700
Temperature (°C)
Heatin
g

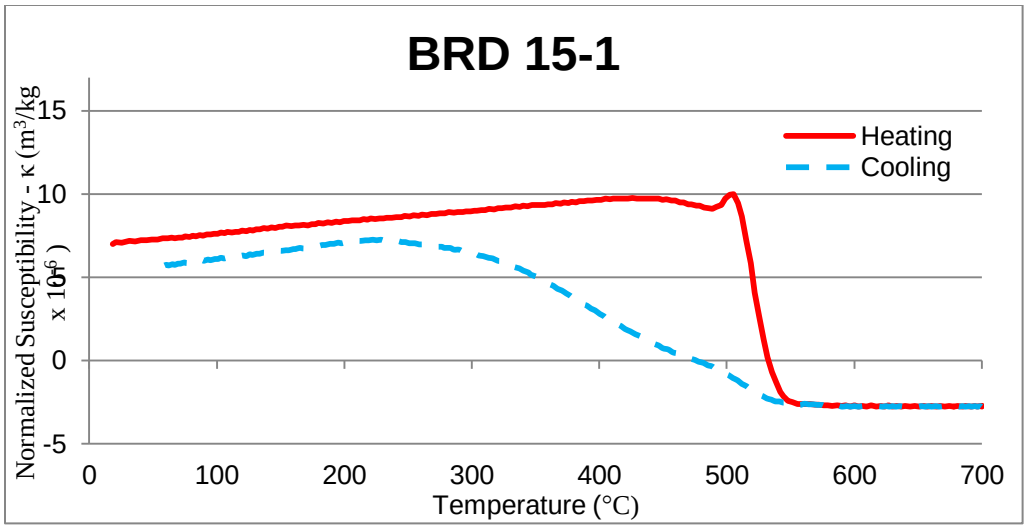
BRD 15-1
Normalized Susceptibility - κ (m³/kg x 10⁻⁶)
15
10
0
-5
0
100
200
300
400
500
600
700
Temperature (°C)
Heating
Cooling

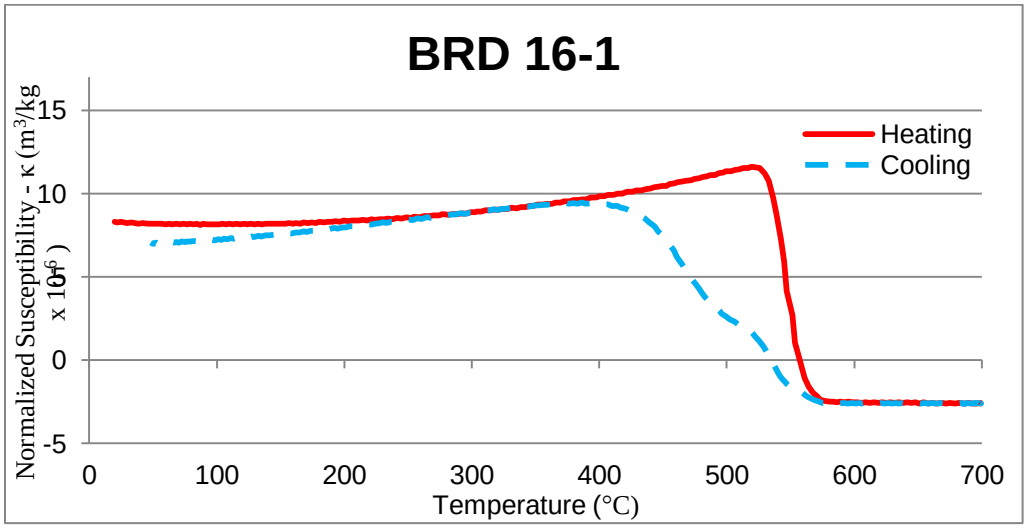
BRD 16-1
Normalized Susceptibility - κ (m³/kg x 10⁻⁶)
15
10
0
-5
0
100
200
300
400
500
600
700
Temperature (°C)
Heating
Cooling

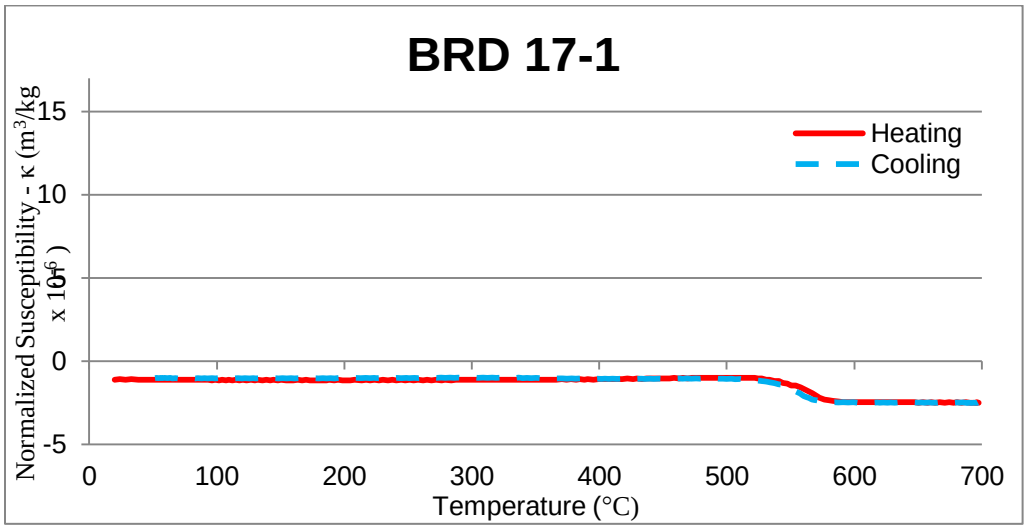
BRD 17-1
Normalized Susceptibility - κ (m³/kg x 10⁻⁶)
15
10
0
-5
0
100
200
300
400
500
600
700
Temperature (°C)
Heating
Cooling

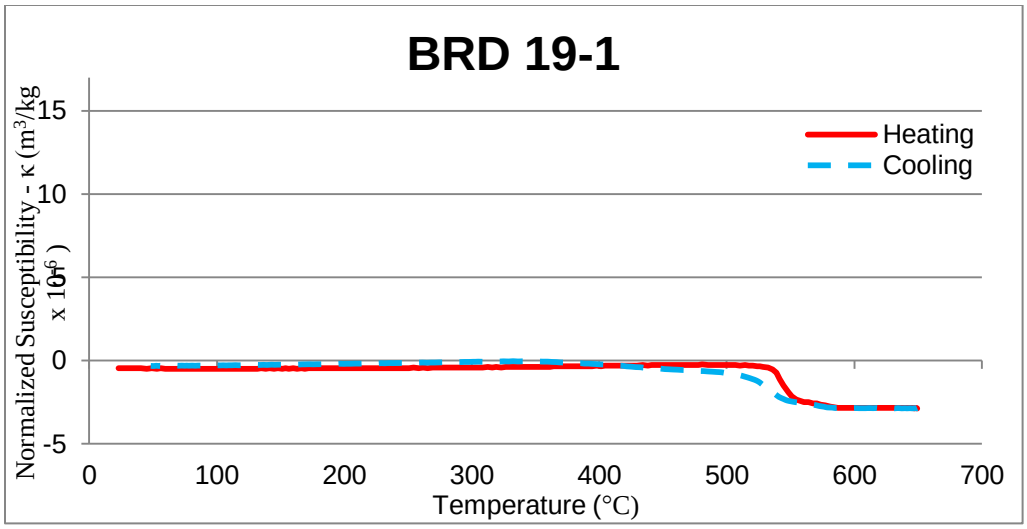
BRD 19-1
Normalized Susceptibility - κ (m3/kg x 10-6)
15
10
0
-5
0
100
200
300
400
500
600
700
Temperature (°C)
Heating
Cooling

REFERENCES

Bilardello, D., Jackson, M.J., 2014, A comparative study of magnetic anisotropy measurement techniques in relation to rock-magnetic properties: Tectonophysics (2014)

Borradaile, G.J., Henry, B., Tectonic applications of magnetic susceptibility and its anisotropy: Earth Science Reviews, v. 42, p. 49-93

Canon-Tapia, E., Herrero-Bervera, E., 2009, Sampling strategies and the anisotropy of magnetic susceptibility of dykes: Tectonophysics, vol. 466, p. 3-27

Chase, C.G., Gilmer, T.H., 1973, Precambrian plate tectonics: the Midcontinent gravity high. Earth Planet Sci Lett., v. 21, p. 70-78

Craddock, J.P., Kennedy, B.C., Cook, A.L., Pawlisch, M.S., Johnston, S.T., Jackson, Mike, 2008, Anisotropy of magnetic susceptibility in Tertiary ridge-parallel dykes (Iceland), Tertiary margin-normal Aishihik dykes (Yukon), and Proterozoic Kenora-Kabetogama composite dykes (Minnesota and Ontario): Tectonophysic, 488, p. 115-124

Davis, D.W., Green, J.C., 1996, Geochronology of the North American Midcontinent rift in western Lake Superior and implications for its geodynamic evolution: Can J. Earth Sci., v. 34, p. 476-488

Dunlop, D.J., 1970, Superparamagnetic and single-domain threshold sizes in magnetite: Journal of Geophysical Research, v. 78, p. 7602, 7613

Dunlop, D.J., 1981, The rock magnetism of fine particles: Physics of the Earth and Planetary Interiors, v. 26, p. 1-26

Dunlop, D.J., Ozdemir, O., Enkin, R.J., 1987, Multidomain and single-domain relations between suseptibility and coercive force: Physics of the Earth and Planetary Interiors, v. 49, p. 181-191

Ellwood, B.B., 1978, Measurement of anisotropy of magnetic susceptibility: a comparison of the precision of torque and spinner magnetometer systems: Journal of Physics E: Scientific Instruments, v. 11, p. 71-75

Herrero-Bervera, E., Walker, G.P.L, Canon-Tapia, E., Garcia, M.O., 2001, Magnetic fabric and inferred flow direction of dikes, conesheets and sill swarms, Isle of Skye, Scotland: Journal of Volcanology and Geothermal Research, v. 106, p. 295-210

Hrouda, F., 1982, Magnetic anisotropy of rocks and its application in geology and geophysics, Geophysical Surverys, v. 5, p. 37-82

Jelinek, V., 1981, Characterization of the magnetic fabrics of rocks: Tectonophysics, v. 79, p T63-T67

Karell, F., Elhers, C., Airo, ML., 2014, Emplacement and magnetic fabrics of rapakivi granite intrusions within Wiborg and Aland rapakivi granite batholiths in Finland: Tectonophysics, v. 614, p. 31-43

Kissel, C., Laj, C., Sigurdsson, H., Guillou, H., 2010, Emplacement of magma in Eastern Iceland dikes: Insights from the magnetic fabric and rock magnetic analyses: Journal of Volcanology and Geothermal Research, v. 191, p. 79-92

Lattard, D., Engelmann, R., Kontny, A., Sauerzapf, U., 2006, Curie temperatures of synthetic titanomagnetites in the Fe-Ti-O system: Effects of composition, crystal

chemistry and thermomagnetic methods: Journal of Geophysical Research, v. 111, no. B12S28

Lu, H., Wang, E., Meng, K., Paleomagnetism and anisotropy of magnetic susceptibility of the Tertiary Janggalsay section (southeast Tarim basin): Implications for Miocene tectonic evolution of the Altyn Tagh Range: Tectonophysics, v. 618 (2014), p. 67-78

Maes, S.M., Tikoff, B., Ferre, E.C., Brown, P.E., Miller, J.D., 2007, The Sonju Lake layered intrusion, northeast Minnesota: Internal structure and emplacement history inferred from magnetic fabrics: Precambrian Research, v. 157, p. 269-288

McEnroe, S.A., Brown, L.L., 2000, A closer look at remanence-dominated aeromagnetic anamoleies: Rock magnetic properties and magnetic mineralogy of the Russel Belt microcline-sillimanite gneiss, northwest Adirondack Mountains, New York: Journal of Geophysical Research, v. 105, no. B7, p. 16,437 - 16,456

Miller, J.D., Chandler, V.W., 1997, Geology, petrology, and tectonic significance of the Beaver Bay Complex, northeastern Minnesota: Geological Society of America, Special Paper 312

Miller, J.D., Green, J.C., Severson, M.J., Chandler, V.W., Hauck, S.A., Peterson, M.D., Wahl, T.E., 2002, Geology and mineral potential of the Duluth complex and related rocks of northeastern Minnesota: Minnesota Geological Survey Report of Investigations, v. 58, p. 207

Morey, G.B., Green, J.C., 1982, Status of the Keweenawan as a stratigraphic unit in the Lake Superior region: See Wold & Hinze, pp. 15-25

Moskowitz, B.M., Hitchhiker's Guide to Magnetism, Environmental Magnetism Workshop 1991, Web Edition

O'Rielly, W., Rock and Mineral Magnetism, 230 pp., Blackie, Glasgow, 1984

Paces, J.B., Miller, J.D., 1993, Precise U-Pb ages of Duluth Complex and related mafic intrusions, northeastern Minnesota: Geochronological insights to physical, petrogenetic, paleomagnetic, and tectonomagmatic processes associated with the 1.1 Ga Midcontinent Rift System: Journal of Geophysical Research, v. 98, no. B8, p. 13,997 - 14,013

Petronis, M.S., Delcamp, A., van Wyk de Vries, B., 2013, Magma emplacement into the Lemptefy scoria cone (Chaine Des Puys, France) explored with structural, anisotropy of magnetic susceptibility, and paleomagnetic data: Bull Volcanol, v.75, p. 753.

Raposo, M.I.B, Enesto, M., 1995, Aniostropy of magnetic susceptibility in the Ponta Grossa dyke swarm (Brazil) and its relationship with magme flow direction: Physics of the Earth and Planetary Interiors (1995), v.87, p. 183-196

Rochette, P., Jackson, M., Aubourg, C., 1992, Rock magnetism and the interpretation of anisotropy of magnetic susceptibility: Reviews of Geophysics, v. 30, no. 3, p. 209-226

Sauvet, C., Gattacceca, J., Rochette, P., Perchiazzi, N., Folco, N., Duprat, J., Harvey, R.P., 2009, Magnetic properties of micrometeorites: Journal of Geophysical Research, v. 114, no. B04102

Soriano, C., Beamud, E., Garces, M., 2008, Magma flow in dikes from rift zones of the basaltic shield of Teneride, Canary Islands: Implications for the emplacement of

buoyant magma: Journal of Volcanology and Geothermal Research, v. 173, p. 55-68

Stein, S., van der Lee, S., Jurdy, D., Stein, C., Weins, D., Wysession, M., Revenaugh, J., Frederiksen, A., Darbyshire., F., Bollmann, T., Lodewyk, J., Wolin, E., Merino, M., Tekverk, K., 2011, Learning from failure: The SPREE Mid-Continent Rift Experiment: GSA Today, v. 21, no. 9, p/ 5-7

Tarling, D.H., Hrouda, F., 1993, The magnetic anisotropy of rocks: Chapman and Hall, London. ISBN: 0412498804

Tauxe, L, Banerjee, S.K., Butler, R.F. and van der Voo R, Essentials of Paleomagnetism, 3rd Web Edition, 2014.

Tauxe, L., Kylstra, N., Constable, C., 1991, Bootstrap statistics for paleomagnetic data: Journal of Geophysical Research B: Solid Earth, v. 96, p. 11723-11740

Tauxe, L., Pick, T., Constable, C., 1996, Wasp-waisted, pot-bellies, and superparamagnetism: Journal of Geophysical Research B: Solid Earth, v. 101, p 571-583, 1996

Van Schmus, W.R., Hinze, W.J., 1985, The Midcontinent Rift System: Annual Reviews in Earth and Planetary Science, v. 13, p. 345-383

Vervoort, J.D., Wirth, K., Kennedy, B., Sandland, T., Harpp, K.S., 2007, The magmatic evolution of the Midcontinent RiftL New geochronologic and geochemical evidence from felsic magmatism: Precambrian Research, v. 157, p. 235-268

ABSTRACT

INVESTIGATING THE ANISTOROPY OF MAGNETIC SUSCEPTIBILITY AND OTHER ROCK MAGNETIC PROPERTIES OF THE BEAVER RIVER DIABASE IN NORTHEASTERN MINNESOTA.

by

SAMER H. HARIRI

December 2014

Advisor: Dr. Sarah Brownlee

Major: Geology

Degree: Master of Science

The Beaver River Diabase (BRD) is a series of mafic dikes and sills within the Beaver Bay Complex (BBC) of northern Minnesota, which formed during the development of the ~1.1 Ga Midcontinent Rift (MCR). The BRD is one of the youngest and most extensive intrusive phases of the BBC. The BRD dikes and sills were emplaced into the medial levels of the 6-10 kilometer-thick North Shore Volcanic Group and occur over an arcuate area extending 120 by 20 kilometers. The BRD is composed of fine- to medium-grained ophitic olivine gabbro and does not display obvious foliation or lineation features and rarely displays modal layering. Without obvious magmatic internal structures, it is difficult to determine emplacement properties such as flow direction using standard geologic mapping or petrographic techniques. For this reason, we measured the anisotropy of magnetic susceptibility (AMS), in conjunction with other rock magnetic properties, to better understand the BRD's emplacement and deformation history in the context of the MCR.

AMS measures the directional dependence of low-field magnetic susceptibility, and is used to infer a shape-preferred orientation of magnetic minerals within a rock, which can be related to specific emplacement mechanisms (e.g. directional flow or settling). Preliminary analysis of AMS at 20 sites within the southern half of the BRD (with 4-7 samples per site) shows maximum susceptibility values between 4.48 x 10^{-6} and 2.22 x 10^{-4} m^3/kg (1165 and 65400 μSI). Most specimens display nearly isotropic AMS ellipsoids (Pj < 1.15) with minor degrees of prolateness and oblateness. However, about 20% of specimens have higher anisotropies (Pj between 1.15 and 1.67) and higher degrees of oblateness and prolateness. Variations in AMS properties may reflect differences in concentration and composition of magnetic minerals, as well as emplacement mechanisms. Measurements of susceptibility as a function of temperature yield Curie points between 470 and 570 °C, indicating the presence of low-titanium titanomagnetite. Major hysteresis loops show coercivities between 1 and 25 mT, consistent with titanomagnetite as the dominant remanence carrier.

Autobiographical Statement

My name is Samer Hariri, a scientist in the making, and an educator at the start of his career. I was born and raised in Beirut, Lebanon, where I spent the first five years of my life amidst a civil war. My family then moved to Riyadh, Saudi Arabia, where I lived and grew up until the year 2003. While in Saudi Arabia, I attended private international schools up until 11th grade. I developed interest in the physical sciences at a young age, primarily in astronomy and geology. I was fascinated by the stars and the planets, and intrigued by volcanoes and fossils. The best gift my parents ever gave me was a set of encyclopedia books of which my favorite two volumes were the books on astronomy and the one on earth science

In 2003, my family and I moved to the United States so that I could continue my upper level education and pursue my dreams. I graduated from North Farmington High School, and attended Oakland Community College. After taking a few physics and astronomy courses and with some advice from my mentor, Dave Stoddard, I decided to major in astrophysics once I transferred to Michigan State University. My goal was to someday become a researcher in the field of planetary formation, but a year before I graduated I discovered geophysics via Dr. Remke Van Dam at the geological science department at MSU. He invited me to go with him to the field where he was conducting groundwater research using electrical resistivity. Being someone who was fond of physics, and who also enjoys the outdoors, I immediately fell in love with this field. I was applying concepts I learned in physics to geological phenomenon, and I was doing science outdoors. I decided to add a major in physics & geophysics that year and it worked out quite nicely as many of my first degree requirements overlapped.

After I graduated from MSU, I wasn't sure in what direction I wanted to go. On one hand, I wanted to do planetary research; on the other, I wanted to work with geophysical related fields. I decided to attend Wayne State University and get my masters in geology and work on a thesis involving rock magnetism. As I near graduation, I feel very fortunate to have been a part of a wonderful geology department that has some of the most inspiring and encouraging faculty I ever met.

My current plan is to teach geology and natural science at the junior college level. However, I still have ambition to pursue my desire to study and conduct research in planetary science. I would like to earn a PhD someday and live out my life doing research and teaching at the college level. Reflecting back on my academic career, the moments I enjoyed the most are those when I was doing research. The process at times felt difficult, but as I became more familiar with it, it became a part of what I was meant to do. For the time being though, I enjoy teaching and will hope to inspire the many students I'll meet just like the many teachers I met have inspired me.